

Unterschrift des Betreuers

DIPLOMARBEIT

Improvement of High Speed Swept Source Optical Coherence Tomography for Optical Angiography

Ausgeführt am

¹Institute of Applied Physics
Vienna University of Technology

²Center for Medical Physics and Biomedical Engineering
Medical University Vienna

Unter der Anleitung von Martin Gröschl¹, Rainer A. Leitgeb², Daniel
Fechtig²

durch

Laurin Ginner

Goldschlagstrasse 88/20, 1150 Wien

Datum

Unterschrift

ABSTRACT

Optical Coherence Tomography (OCT) is an established optical imaging technique for non-invasive medical diagnosis with many different medical applications. One of the most important functional extensions of OCT is label-free retinal angiography based on speckle variance, because it is non-invasive and very fast compared to the common fluorescence angiography techniques. In ophthalmology it is of interest to analyze the retinal microvascular structure, because there are a number of diseases associated with it. This thesis aims to improve angiography of the human retina based on an existing dual beam swept source OCT device operating at 1050nm central wavelength. In optical angiography it is of importance to enlarge the field of view (FOV) without degrading the microvascular resolution by motion artifacts and insufficient sampling of the object. Common OCT systems are limited by their imaging speed to small regions of around 8° FOV. To increase the imaging speed a number of hardware and software techniques are proposed. The increased imaging speed enables faster scanning and therefore a bigger FOV, which is verified experimentally in this thesis.

ZUSAMMENFASSUNG

Optische Kohärenz Tomografie ist eine weit verbreitete Technik zur optischen Bilderfassung. Es gibt viele verschiedene Anwendungsmöglichkeiten für OCT im medizinischen Bereich. Eine der wichtigsten funktionellen Erweiterungen von OCT ist retinale Angiographie, weil sie sehr schnell und nicht invasiv im Vergleich zu den weit verbreiteten Fluoreszenz Verfahren ist. Diese Arbeit behandelt retinale Angiographie mit einem bereits existierendem OCT Gerät. Das verwendete System in dieser Arbeit ist ein Zweistrahl-OCT Gerät, welches die Bestimmung des Blutflusses und der Angiographie gleichzeitig ermöglicht. Die Lichtquelle ist ein Swept Source Laser mit einer zentralen Wellenlänge von 1050 nm. Für Mediziner ist es von besonderem Interesse die retinale microvaskuläre Struktur zu studieren um etwaige Krankheiten zu erkennen und zu beobachten. Die optische Angiographie wird verwendet um diese microvaskulären Strukturen zu erfassen. Wichtig ist dabei die Erfassung eines großen Bereichs der Retina ohne dabei die Auflösung der kleinen Strukturen durch zu grobes sampeln oder durch Bewegungsartefakte zu verlieren. Konventionelle OCT Systeme haben eine durchschnittliche Bereichserfassung von 8° , welche limitiert ist durch die Geschwindigkeit der Messung. Um die Geschwindigkeit der Datenerfassung zu erhöhen werden in dieser Arbeit verschiedene Techniken vorgestellt. Höhere Geschwindigkeit ermöglicht das Vermessen eines größeren retinalen Bereichs. Ziel ist es den Erfassungsbereich auf 16° zu verdoppeln und experimentell zu verifizieren, dass dabei die mikrovaskuläre Struktur nicht verloren geht.

TABLE OF CONTENTS

| Chapter | Page |
|---|------|
| 1 INTRODUCTION..... | 9 |
| 2 BACKGROUND AND LITERATURE REVIEW..... | 13 |
| 2.1 Optical Imaging systems | 13 |
| 2.2 Optical Coherence Tomography..... | 15 |
| 2.2.1 Time domain OCT (TD-OCT):..... | 18 |
| 2.2.2 Fourier domain OCT (FD-OCT):..... | 18 |
| 2.2.3 Spectral domain OCT (SD OCT)..... | 19 |
| 2.2.4 Swept source OCT (SS OCT) | 19 |
| 2.3 Interferometer | 21 |
| 2.4 Lateral resolution..... | 26 |
| 2.5 Axial resolution | 26 |
| 2.6 Image-SNR | 27 |
| 2.7 Doppler OCT | 28 |
| 2.8 Angiography | 31 |
| 2.9 The human eye..... | 33 |
| 2.10 The retina..... | 34 |
| 2.11 Remapping..... | 36 |
| 2.12 Errors | 37 |
| 2.12.1 Dispersion | 37 |
| 2.12.2 Crosstalk..... | 37 |
| 2.12.3 Motion artifacts | 38 |
| 3 METHODOLOGY | 39 |
| 3.1 System Setup | 39 |
| 3.2 Multiplexed Laser Source..... | 41 |
| 3.3 High Speed Galvo Scanner..... | 42 |
| 3.4 Spectral Splitting | 43 |
| 3.5 Bulk motion compensation..... | 45 |
| 3.6 Angular compounding | 46 |
| 3.7 Flattening of the Tomogram..... | 47 |
| 3.8 In Vivo Measurement Protocol | 48 |
| 4 RESULTS..... | 49 |
| 4.1 Multiplexed Laser..... | 49 |
| 4.2 High Speed Galvo Scanner..... | 50 |
| 4.3 Spectral Splitting | 51 |

| | | |
|-----|---------------------------|----|
| 4.4 | Angular Compounding | 57 |
| 4.5 | Case of Pathology | 59 |
| 5 | CONCLUSION | 61 |
| 6 | OUTLOOK..... | 63 |
| 7 | REFERENCES..... | 64 |
| 8 | APPENDIX | 66 |

LIST OF EQUATIONS

| | |
|---|----|
| EQUATIONS 1, INTENSITY PROPORTIONAL TO REFERENCE AND SAMPLE FIELD. FORM [1] | 16 |
| EQUATION 2, POLYCHROMATIC PLANE WAVE. | 21 |
| EQUATION 3, SERIES OF SAMPLE DELTA FUNCTIONS. | 21 |
| EQUATION 4, REFLECTED BEAM FOR THE SAMPLE. | 21 |
| EQUATION 5, INTENSITY OF INTERFERED SIGNAL. | 22 |
| EQUATION 6, DETECTOR SIGNAL. FROM [1] | 22 |
| EQUATION 7, GAUSSIAN FUNCTION OF A LIGHT SOURCE SPECTRUM. | 22 |
| EQUATION 8, CONVENTION FOR FOURIER TRANSFORMATION. | 23 |
| EQUATION 9, CONVOLUTION PROPERTY OF FOURIER TRANSFORMATION. | 23 |
| EQUATION 10, DETECTOR SIGNAL AFTER DELTA SHIFTING. | 23 |
| EQUATION 11, LATERAL RESOLUTION. | 26 |
| EQUATION 12, AXIAL RESOLUTION. | 26 |
| EQUATION 13, SIGNAL-TO-NOISE RATIO FROM REFERENCE TO TEST IMAGE. | 27 |
| EQUATION 14, INTENSITY AND PHASE OF THE INTERFEROGRAM. FROM [8] | 28 |
| EQUATION 15, VELOCITY OF PARTICLES IN Z DIRECTION. FROM [8] | 28 |
| EQUATION 16, ABSOLUTE VELOCITY. FROM [8] | 28 |
| EQUATION 17, ANGLE INDEPENDENT DUAL BEAM VELOCITY. FROM [10] | 29 |
| EQUATION 18, TOTAL BLOOD FLOW. FROM [9] | 29 |
| EQUATION 19, INTERFEROGRAM, LOGARITHMICALLY SCALED. FROM [11] | 32 |
| EQUATION 20, SPECKLE VARIANCE. FROM [11] | 32 |
| EQUATION 21, THRESHOLDING. FROM [11] | 32 |
| EQUATION 22, SUMMATION OF SPECKLE VARIANCE. FROM [11] | 32 |
| EQUATION 23, TOMOGRAMS LOGARITHMICALLY SCALED. SELF-GENERATED | 44 |

ABBREVIATIONS

| | |
|-------------|--------------------------------|
| OCT | Optical Coherence Tomography |
| FFT | Fast Fourier Transformation |
| FD-OCT | Fourier Domain OCT |
| TD-OCT | Time Domain OCT |
| SD-OCT | Spectral domain OCT |
| SS-OCT | Swept source OCT |
| SV-OCT | Speckle variance OCT |
| D-OCT | Doppler OCT |
| CCD | Charge-coupled device |
| SNR | Signal to noise ratio |
| NA | numerical Aperture |
| FOV | Field of View |
| RPE | Retinal Pigment Epithelium |
| CNV | Choroidal neovascularization |
| FWHM | Full width at half maximum |
| Kerr-effect | quadratic electro-optic effect |

LIST OF FIGURES

| Figure | Page |
|---|------|
| FIGURE 1, COMPARISON OF IMAGING TECHNIQUES. THE AXIAL RESOLUTION OF OCT IS FROM 1 TO 15 μM , THE IMAGING DEPTH IS LIMITED TO 3 MM DUE TO OPTICAL SCATTERING. FROM [1] | 14 |
| FIGURE 2 SCHEMATIC OF THE FUNCTION PRINCIPLE OF AN OCT DEVICE. THE PLANES ON THE RIGHT SIDE ARE DIFFERENT REFLECTION DEPTHS OF THE SAMPLE BEAM. AFTER INTERFERENCE WITH THE REFERENCE BEAM THE SIGNAL GETS DETECTED WITH A PHOTODIODE. FROM [3] | 16 |
| FIGURE 3, SHOWS THE DIFFERENT INFORMATION OF A SINGLE POINT SCAN WHICH CONTAINS THE DEPTH INFORMATION (A-SCAN), THE TRANSVERSE SCAN WHICH MEANS A 1D LINE OFFERING A SERIES OF A-SCANS IN ONE DIRECTION FORMING A SO CALLED B-SCAN AND A WHOLE 3D STACK SCANNING IN TWO DIRECTIONS FORMING A COMPLETE VOLUME. FROM [1] | 17 |
| FIGURE 4, SHOWS THE SCHEMATICS OF TD-OCT USING A BROAD BANDWIDTH LIGHT SOURCE AND SCANNING WITH THE REFERENCE MIRROR, THE SCHEMATICS OF AN SS-OCT SYSTEM USING A SWEEP SOURCE WHICH SCANS THROUGH A SET OF FREQUENCIES AND FORMS A TIME CORRELATION TO EACH FREQUENCY, AS WELL AS THE SCHEMATIC OF AN SD-OCT SYSTEM WHICH USES A BROAD BANDWIDTH LIGHT SOURCE AND A SPECTROMETER TO DISTINGUISH DIFFERENT FREQUENCIES. FROM [6] | 20 |
| FIGURE 5, SHOWS THE INTERFEROMETRIC SIGNAL FOR A SINGLE SAMPLE REFLECTOR FORMING A COSINE STRUCTURE OF THE INTERFEROMETRIC SIGNAL (LEFT). FOR MORE REFLECTION IN THE SAMPLE WE GET A FULL MODULATION OF COSINE FUNCTIONS (RIGHT). THE AMPLITUDE OF THE LEFT IMAGE IS CORRESPONDS TO THE DC AMPLITUDE, THE SMALL AMPLITUDE OF THE MODULATION TO THE CROSS-CORRELATION AMPLITUDE. FROM [1] | 24 |
| FIGURE 6, SHOWS DE DIFFERENT TERMS WHICH RESULT FROM EQN. 10, FROM TWO DELTA REFLECTIONS FROM THE SAMPLE TISSUE. FROM [1] | 24 |
| FIGURE 7, SHOWS THE SIGNAL WHICH IS DETECTED AT THE PHOTODETECTOR, IN THE MIDDLE THERE IS THE DC-TERM OF THE REFERENCE BEAM, THE AUTOCORRELATION TERM SHOWS THE SELF-INTERFERENCE OF THE BACKSCATTERED LIGHT, AND THE CROSS CORRELATION WHICH CONTAIN THE STRUCTURAL INFORMATION. FROM [6]..... | 25 |
| FIGURE 8, SHOWS THE DOPPLER ANGLE α BETWEEN THE LASER BEAM AND THE BLOOD VESSELS AS WELL AS THE ANGLE BETWEEN THE TWO BEAMS k_A AND k_B $\Delta\alpha$. IN THE FUNDUS PROJECTION, THE VESSELS HAVE AN ANGLE β AND THE PLANE OF THE TWO BEAMS AN ANGLE $\Delta\beta$ TO THE SCANNING COORDINATES. FROM [9] | 30 |
| FIGURE 9, SHOWS THE INTERNAL STRUCTURE OF A HUMAN EYE, THE CORNEA AND THE SCLEAR FORM THE OUTER PART OF THE EYE, THE IRIS, CHOROID AND CILIARY BODY THE SECOND LAYER AND THE RETINA THE INNERMOST LAYER, WHICH HOLDS THE PHOTORECEPTORS. FROM [12] | 33 |
| FIGURE 10, SHOWS THE DETAILED STRUCTURE OF THE RETINA AT THE FOVEA REGION. SELF-GENERATED.... | 34 |
| FIGURE 11, SHOWS THE DETAILED STRUCTURE OF THE RETINA AROUND THE ONH. SELF-GENERATED | 35 |
| FIGURE 12, SHOWS THE RESULT OF NO PROPER REMAPPING, A BROADENING OF THE DEPTH STRUCTURE IS VISIBLE WHICH DESTROYS THE EXACT DEPTH POSITION. FROM [14] | 36 |
| FIGURE 13, SHOWS THE SCHEMATIC OF THE OCT-SETUP. THE RED AND BLUE LINE CHARACTERIZING A AND B BEAM. FROM [10]..... | 39 |
| FIGURE 14, SHOWS THE SWEEP STRUCTURE OF THE NEW AXSUN LASER. SELF-GENERATED | 41 |
| FIGURE 15, SHOWS THE SPLIT SPECTRA APPROACH. SELF-GENERATED | 43 |

FIGURE 16, SHOWS THE 8° SECTION AROUND THE FOVEA WITH 100 KHZ ON THE LEFT SIDE AND IN COMPARISON THE 8° SECTION OF THE FOVEA WITH 200 KHZ. SELF-GENERATED 49

FIGURE 17, SHOWS THE NEW IMAGES MADE WITH THE CAMBRIDGE SCANNER IN COMPARISON WITH THE OLD ONES WITH THE THORLABS SCANNER. ON THE LEFT SIDE ARE THE NEW IMAGES WITH 16° AT THE FOVEA AND THE ONH. ON THE RIGHT SIDE ARE THE IMAGES WITH THE OLD SCANNER AT NEARLY THE SAME POSITION. AS CAN BE SEEN WITH THE NEW SCANNER MORE STRUCTURAL DETAILS ARE VISIBLE. 50

FIGURE 18, (A) SHOWS AN 8° SECTION AROUND THE FOVEA WITH A STANDARD 100 KHZ SYSTEM, (B) SHOWS THE RESULT WITH THE NEW MULTIPLEX LASER WORKING AT 200 KHZ AND (C) SHOWS THE SAME AREA WITH THE MULTIPLEX SPLIT SPECTRA REACHING VIRTUAL 400 KHZ. SELF-GENERATED 51

FIGURE 19, (A) SHOWING A 8° SECTION AROUND THE FOVEA WITH A STANDARD 100 KHZ SS-OCT. (B) SHOWS THE 16° DOUBLE FOV WITH THE 400 KHZ APPROACH, IN (C) THE 8° SECTION OF THESE 16° IMAGE CAN BE SEEN, WHICH SHOWS REMARKABLY THE SAME STRUCTURE AND EVEN A BETTER SNR. SELF-GENERATED 53

FIGURE 20, (A) SHOWS THE 16° FOVEA SECTION WITH THE MULTIPLEX 200 KHZ, IN COMPARISON WITH THE (B) 16° DOUBLE SPLIT TECHNIQUE. (C) AND (D) SHOWS THE YELLOW SUBSECTION OF (A) AND (B) TO CLARIFY THE QUALITY INCREASE. (E) SHOWS THE LINE PLOT OF THIS SUBSECTION (YELLOW LINE) A REMARKABLE INCREASE IN SNR IS VISIBLE. SELF-GENERATED..... 54

FIGURE 21, (A) SHOWS THE 16° ONH SECTION WITH 200 KHZ AND (B) WITH THE DOUBLE SPLIT 400 KHZ. AS WELL THERE ARE SUBSECTIONS TO SHOW THE INCREASE IN SNR (A') AND (B'). (C) SHOWS THE LINE PLOT, AGAIN AN INCREASE IN SNR IS VISIBLE. SELF-GENERATED 55

FIGURE 22, SHOWS THE INCREASE IN MICROVASCULAR STRUCTURE CONTRAST FOR AN IMAGE OF 8° ACROSS THE FOVEA, USING ANGULAR COMPOUNDING. THE IMAGES OF THE TWO DIFFERENT BEAMS ARE PLOTTED IN THE LEFT COLUMN. EACH BEAM OFFERS A SLIGHTLY DIFFERENT ANGLE TO THE FOVEA, RESULTING IN DIFFERENT SPECKLE PATTERNS. SUMMATION AVERAGES SPECKLE, WHICH IMPROVES STRUCTURAL DETAILS IN THE COMPOUNDED IMAGE. 57

FIGURE 23, SHOWS THE INCREASES IN MICROVASCULAR STRUCTURE FOR A IMAGE AT 16° FOVEA SECTION, FORM THE TWO DIFFERENT BEAMS, EACH BEAM OFFERS A SLIGHTLY DIFFERENT VISION TO THE FOVEA WHICH IMPROVES STRUCTURAL DETAILS IN THE COMPOUNDED IMAGE. 58

FIGURE 24, SHOWS THE ONH AND THE FOVEA OF A CNV PATHOLOGY, AT THE FOVEA A NEOVASCULARIZATION IS VISIBLE (GREEN). SELF-GENERATED 59

1 INTRODUCTION

Optical Coherence Tomography (OCT) is an optical imaging technique based on low coherence interferometry. With OCT a full 3D tomogram of a biologic sample can be acquired non-invasively. Therefore it is of great interest to medicine and in broad use especially in ophthalmology. Due to the transparency of the eye, OCT can be used for imaging the retinal structure in high speed and high resolution. This makes OCT one of the leading technologies in detection of eye diseases, affecting the retinal structure and its properties. One of the most important applications of OCT imaging is label-free retinal optical angiography based on speckle variance, because it is non-invasive and very fast compared to the common fluorescence angiography techniques.

In this thesis we cover two extensions of OCT, one is Doppler OCT (D-OCT), which enables blood flow measurements in retinal vessels. Blood flow in the retina is altered in specific diseases, which makes proper detection of quantitative blood flow a main goal for D-OCT. State of the art D-OCT systems are using two beams to allow angle independent blood flow measurement. The measurements in this thesis are based on a swept source OCT system employing a dual beam rotation system which offers angle and plane independent blood flow detection in the retina.

A second extension of OCT is retinal angiography, which allows to detect the vessel structure of the retina non-invasively. State-of-the-art techniques use a contrast agent for fluorescence angiography which is time-consuming, invasive and offers only two-dimensional information. OCT angiography in contrast offers a way to detect the microvascular structure non-invasively. However, current OCT angiography systems have limited number of sampling points due to the slow imaging speed. Only proper sampling offers the microvascular structure. Furthermore, to minimize the influence of motion artifacts, the measurement of a human eye should be below 10 sec. Current optical angiography OCT systems therefore offer a field of view (FOV) limited to around 8° , which corresponds to 2.3mm. To get a higher FOV the sampling speed has to be increased.

This was the main aim of this work. Several implemented techniques are described below, which increase the scanning speed of an already existing swept source dual beam OCT device. We first increase the sweeping speed with a new laser operating at 200kA-scans/s. As a second step we introduce a method based on spectral splitting for a virtual increase in lateral sampling

points to enable a further increase in FOV without losing structural information. As a third step, we introduce angular compounding of the two beams, which combines the two recorded images of beam 1 and 2 of the dual beam system. All these steps should guarantee the same resolution while increasing the FOV by a factor of 2 to 16° or 4.6mm.

Chapter 2 describes the background and physical principles which are used to acquire the OCT data necessary to obtain the final OCT angiography images. A short introduction to optical imaging systems and the different types of OCT-devices is given. The theory of interferometry and important system parameters are discussed as well as the human eye.

In **Chapter 3** the setup and the processing steps developed in this work are explained (swept source OCT setup, multiplex Laser, split spectra method, angular compounding). To demonstrate the feasibility of the implemented techniques, **Chapter 4** offers the experimental results of optical angiography performed with a healthy human volunteer. Finally, **Chapter 5** and **6** sum up the results and give a short outlook on future work.

EINLEITUNG

Optische Kohärenz Tomographie (OCT) ist ein bildgebendes Verfahren, welches mittels Interferenz funktioniert. Mit OCT kann man ein ganzes 3D Tomogramm von biologischen Proben erfassen ohne Kontrastmittel verwenden zu müssen. Deshalb ist OCT von großem Interesse für die Medizin und weit verbreitet, vor allem in der Augenheilkunde. Wegen der Transparenz des Auges ist OCT einsetzbar um die Struktur der Retina sehr schnell und in hoher Auflösung zu erfassen. Dies macht OCT zu einem der führenden Verfahren um Augenkrankheiten und deren Einfluss auf die retinale Struktur zu erfassen.

In dieser Arbeit befassen wir uns mit 2 Verfahren von OCT, erstens Doppler OCT, welches die Erfassung des Blutflusses in der Retina ermöglicht. Der retinale Blutfluss wird von Krankheiten verändert, deshalb ist eine gute Bestimmung dieses Flusses das Hauptziel von Doppler OCT. Doppler OCT erfasst Bewegungen innerhalb des Auges hervorgerufen durch den Blutfluss, somit lässt sich dessen Fließgeschwindigkeit ermitteln. Heutzutage verwendete Systeme basieren auf zwei Strahlen um winkelunabhängig zu messen. Unser System rotiert diese Strahlen zusätzlich, welche winkel- und ebenenunabhängige Blutflussanalyse garantiert.

Das zweite Verfahren ist die retinale Angiographie, welche die Gefäßstruktur der Retina zeigt. Viele Krankheiten verändern diese Struktur. Heutzutage verwendete Systeme zur Erfassung der retinalen Gefäßstruktur injizieren fluoreszierende Kontrastmittel, was zeitaufwändig und invasiv ist. OCT Angiographie ist ein möglicher Weg um mikro-vaskuläre Strukturen in der Retina nichtinvasiv zu erfassen. State-of-the-art OCT Systeme haben eine limitierte Anzahl von Samplingpunkten, welche von der Aufnahmegeschwindigkeit des Systems abhängen. Nur ein ausreichendes Sampling garantiert die Visualisierung von mikrovaskulären Strukturen. Bei der Diagnose des menschlichen Auges sollte die Messdauer unter 10 sec. sein, um etwaige Artefakte durch Augenbewegungen zu reduzieren und Zwinkern zu vermeiden. Dadurch ist der Messbereich (engl. Field of view) auf ca. 8° (2.3mm) begrenzt. Um größere Messbereiche vernünftig zu sampeln muss man die Aufnahmegeschwindigkeit des Systems erhöhen.

Das Hauptziel dieser Arbeit war daher, Methoden zu entwickeln um die Geschwindigkeit eines bereits existierenden Zweistrahl-OCT Systems zu erhöhen. Zuerst erhöhten wir die Geschwindigkeit mittels eines neuen, schnelleren Lasers und als zweiten Schritt führten wir eine Technik namens „Split-Spektrum“ durch, welche zusätzlich die Geschwindigkeit um einen Faktor 2 erhöht. Um die 2 Strahlen effektiv zu nutzen führten wir weiters eine

Technik ein, welche sich „Angular Compounding“ nennt, dabei werden die Bilder beider Strahlen verwendet. All diese Schritte sollen es ermöglichen den Messbereich von ursprünglich 8° auf 16° (4.2 mm) in beide Richtungen bei gleichbleibender Auflösung der Gefäßstruktur zu verdoppeln. **Kapitel 2** beschreibt den theoretischen Hintergrund, wie die Bilddaten gemessen und verarbeitet werden. Zusätzlich werden die verschiedenen Typen von OCT-Systemen kurz erklärt. **Kapitel 3** umfasst den Methodenteil, welcher einen kurzen Überblick über die Eigenschaften des verwendeten OCT Systems liefert und eine detaillierte Beschreibung der verwendeten Schritte beinhaltet welche zur Vergrößerung des Messbereiches führen. Um die Änderungen zu quantifizieren werden im **Kapitel 4**, die Resultate an einem gesunden Auge eines Probanden verglichen. Am Ende in **Kapitel 5** und **6** werden die Resultate kurz zusammengefasst und ein kurzer Ausblick betreffend zukünftiger Verbesserungen und Applikationen gegeben.

2 BACKGROUND AND LITERATURE REVIEW

To understand how exactly a SS-OCT System works, a short description of the development of OCT, Fourier Domain Interferometry and resolution follows.

2.1 Optical Imaging systems

There are several different types of optical imaging systems for biological samples, such as microscopy, ultrasound or X-ray techniques. The oldest and best known is standard microscopy which works with light in the visible range and has a high resolution of 1 μm and below. However, it has the disadvantage that visible light is highly scattering and thus only surface structure with a depth of about hundred μm and less is visible. For better depth information another technique must be used. X-ray techniques on the other hand are used to scan through the whole biological sample due to the high energy level of the beams, but have the disadvantage of causing ionization and therefore are harmful to biological samples. Furthermore not all biological structure is visible with X-ray, as it's scattering at elements with a higher atomic number, which makes organs hard to visualize but shows the bone structure for example. The use of a contrast medium is necessary to get a more specific information of organic structure. A way to overcome these problems is ultrasound, which uses high frequency sound waves to detect internal structure; these sound waves are transmitted with a low absorption and it's possible to image up to several cm into a sample. Such techniques are widely used for pre natal diagnosis or visualization of soft parts such as kneecaps. A disadvantage is that the resolution is around 100 μm and it is not suitable for every sample (eye). Modern high frequency ultrasound has reached resolutions up to 15 μm with frequencies up to 100MHz and more. These frequencies are highly absorbed with depth, therefore a depth penetration of only some mm are possible. The technique to close the gap between microscopy and ultrasound is optical coherence tomography (OCT). Modern techniques reach a resolution around 1-10 μm , which is a clear increase compared to normal ultrasound. OCT uses light in the near infrared and has a depth penetration of up to 3 mm. The OCT-technique is similar to ultrasound but uses light instead of sound waves. The essential point is to measure the intensity and echo time of reflected light from the sample compared to a reference signal. This technique offers a wide range of use such as high resolution imaging of the eye, scanning of melanomas and nondestructive testing applications for electronic products.

As OCT is an optical technique it can be combined with other instruments, endoscopes or needles, to image internal parts of the body.

Figure 1 shows the resolution and image depth of different visualization techniques for medical issues.

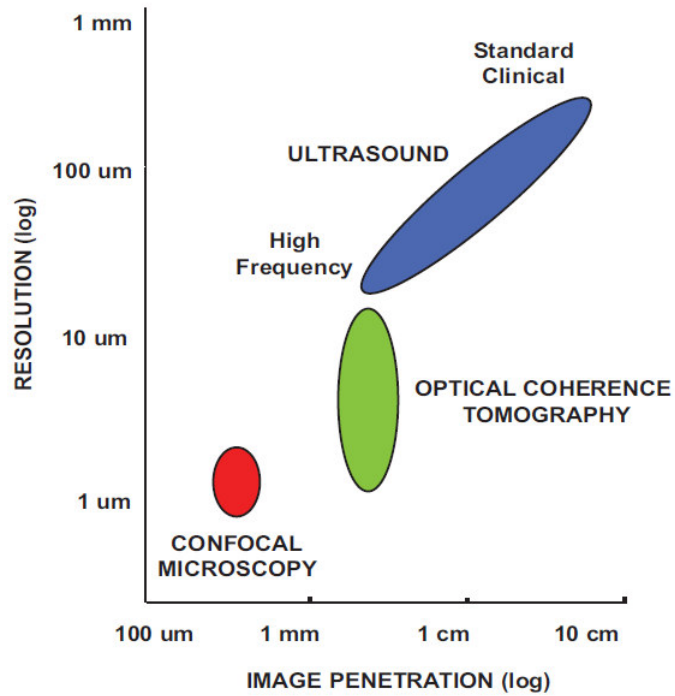


Figure 1, Comparison of imaging techniques. The axial resolution of OCT is from 1 to 15 μm, the imaging depth is limited to 3 mm due to optical scattering. From [1]

2.2 Optical Coherence Tomography

The basic technique for OCT is measuring the time delay between reference and sample reflection. The first publication regarding photographing light in flight was proposed in 1971 by Michel Duguay [2]. In the experiment an ultrafast shutter on the basis of the Kerr effect¹ was used to measure time delay of light. This shutter works with an intense light pulse to induce the Kerr effect in an optical medium. Such shutter can reach extremely high response time up to pico- or femtoseconds. With this extremely high velocity shutter unwanted scattered light can be reduced and enables detection of light echoes from tissues. It appeared rather difficult to ensure such high velocity shutters due to the need of high intensity short laser pulses, which were used to induce the Kerr effect. Such time domain setups achieved a sensitivity of around -70dB, which is not enough to image most biological samples.

A new technique came up to measure the time delay not directly by time, instead using coherent light to enable interferometry. Interferometry appeared to be the ideal technique for measuring the intensity and the time delay of backscattered light with high sensitivity. The principle of OCT is to use low coherent light for interferometry between the reflected sample light and a reference beam. Interference is only possible if the length of the reference beam is nearly equal to the length of the sample beam, which means that the light is still coherent. The interference signature offers information about the depth profile of the sample. The light is reflected from the sample by the diversity of different media, and the change of the refractive index n . Interferometry detects the amplitude of light rather than its intensity.

The OCT process is similar to supersonic, but using light instead of sound waves. In ultrasound techniques the time delay between the outgoing and reflected wave is measured and therefore the internal structure can be determined. Light has a velocity in vacuum of 299 792 km/s, which makes measurement of time delay corresponding to distances of a few micrometers currently impossible. Interferometry is more sensitive to this minimal time delays caused by different reflection- and path lengths in the sample. After interference with the reference beam with a known length the internal structure of the sample can be determined. Nowadays OCT systems achieve a sensitivity of more than -100dB, which is enough for most biological tissues to measure in vivo.

¹ The Kerr effect, is the change of the refractive index due to the application of an electric field.

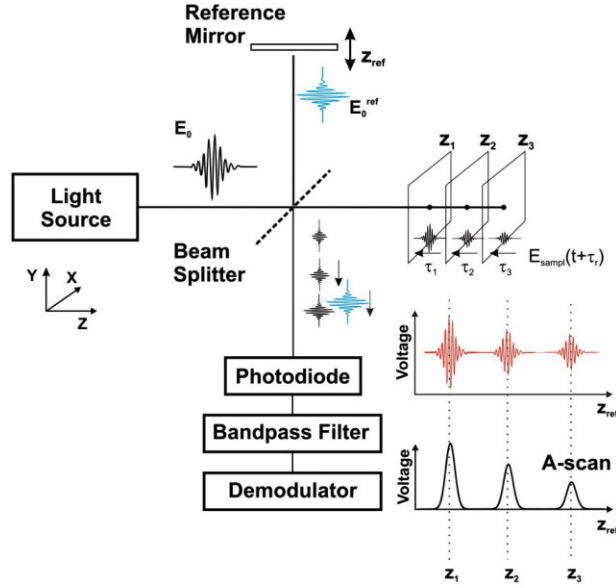


Figure 2 Schematic of the function principle of an OCT device. The planes on the right side are different reflection depths of the sample beam. After interference with the reference beam the signal gets detected with a photodiode. From [3]

Figure 2 shows the schematic function of an OCT device. The light from the source gets split in a beam splitter. One beam goes to a reference mirror with a known path length and the second gets transmitted towards the sample. This is also the basic construction of a Michelson Morley interferometer. The light which travels towards the reference mirror can be described as $E_r(t)$ and the sample beam as $E_s(t)$. The electric field at the photodiode can be described as a function of E_r and E_s . The intensity measured at the detector is proportional to the square of the total field and has a cosine fluctuation.

$$I_0 \sim |E_r|^2 + |E_s|^2 + 2E_r E_s \cos(2k\Delta L)$$

Equations 1, Intensity proportional to reference and sample field. Form [1]

The different z in Figure 2, are different reflection depths from the sample, these different depths form the ΔL in comparison with the reference path length. The reflected sample beam gets interfered with the reference beam, and forms an interferogram at the detector (photodiode). If a long coherent light source is used, interference over a wide range of the path length can be detected. To get to the exact position of the optical echo from the sample beam a low-coherence light source is required. With low coherence light, interference can only be observed when the path lengths from reference and

sample matches within this coherence length, which therefore should be short for a good depth localization. From this interferogram the depth structure can be calculated.

The use of a galvo scanner offers the possibility to scan over an area and to acquire a whole 3D Stack of the sample. A single point scanned with a laser forms a so called A-scan, which is the depth information of one single spot (Figure 3, left image). Performing a line scan forms a so called B-scan which contains the depth information (A-scan) over a 1 D line, which forms a 2D image as can be seen in the central image in Figure 3. Combined with a second scanner offers a full 3D image (tomogram) of a sample, also shown in the right image in Figure 3.

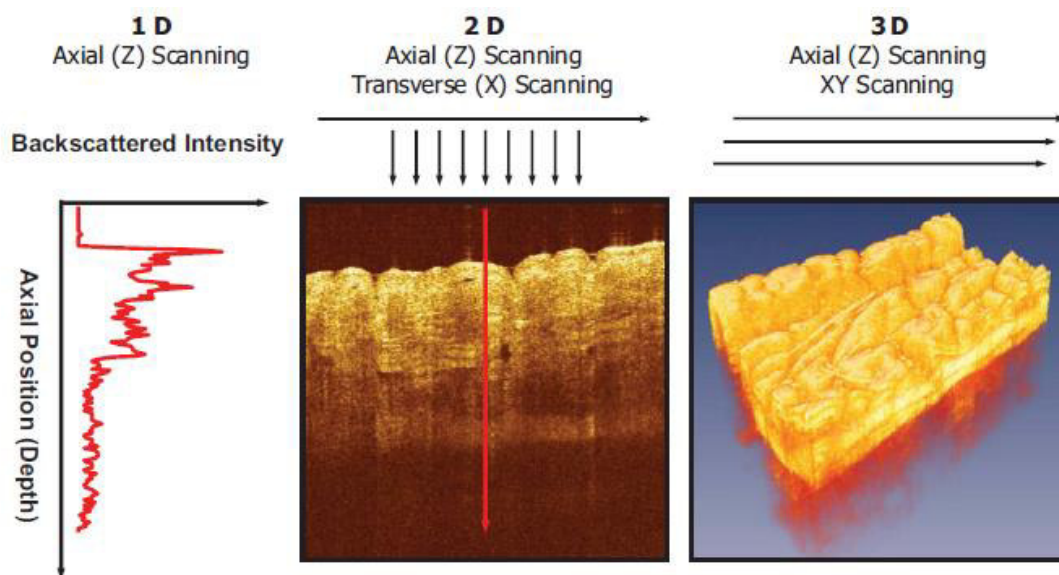


Figure 3, shows the different information of a single point scan which contains the depth information (A-scan), the transverse scan which means a 1D line offering a series of A-scans in one direction forming a so called B-scan and a whole 3D Stack scanning in two directions forming a complete volume. From [1]

First OCT imaging was demonstrated in 1991 by David Huang [4]. The first OCT system used laser with a wavelength of 830nm and achieved an axial resolution of 15 μm . The further development of OCT was fast with the first in vivo image in 1993 by Fercher [5]. OCT became the system in ophthalmology to detect early stages of diseases before physical symptoms an irreversible vision loss occurs. Also the disease monitoring of the effectiveness of treatments can be easily made, due to its fast and non-invasive character.

There are two main principles of OCT-systems.

2.2.1 Time domain OCT (TD-OCT):

This principle operates in direct depth-space z in relation to the reference mirror position. A full A-scan containing the depth information of the sample structure is recorded by measuring the interference signal while the reference arm is moved in axial direction at constant speed. The time delay between reference and sample arm is measured forming an interferogram which is detected by a photodetector. Interference can be observed each time when the path length difference between the backscattered sample field from a specific depth location and the reference arm field is smaller than the coherence length of the light. For each reference length the whole intensity of the beam is acquired. This measurement technique is time consuming and the SNR is rather bad due to mechanical movement, which generates vibrations that disturbs the sensitivity.

2.2.2 Fourier domain OCT (FD-OCT):

This principle operates in spectral domain, instead of the time dependent interferogram in TD the cross-power spectrum of the interfered reference and sample beam is detected. This means the FD OCT detects not the optical power, instead the optical energy is detected. A spectrometer or time separation between the different wavelengths is used to record the spectral interference pattern. Due to the Wiener_Khinchin Theorem², the depth structure can be directly determined via the Fourier transformation of the spectra. Therefore no movement in the reference arm is needed, and it's up to 100 times faster than TD-OCT. Providing a faster acquisition of data FD-OCT is used for scanning of human samples, because longer exposure times of the sample induces motion, which reduces sensitivity. FD-OCT offers at one position an A-scan in a single exposure, which means the depth information for one point at the sample. Cross-sectional images can be generated by scanning with galvo scanners and getting a series of A-scans at different positions. Using of a second scanner allows generating a 3D image.

² The Wiener Khinchin Theorem, states the relation between auto correlation and spectral power density.

The technique further used in this paper is Fourier domain (FD). FD OCT technique can be divided in two sections.

2.2.3 Spectral domain OCT (SD OCT)

A broadband light source in continuous mode is used in combination with a spectrometer, or wavelength sensitive detector. Mostly used is a grating and line CCD camera. Each spot on the line CCD corresponds to a distinct frequency of the spectra, which is selected by the grating properties of the spectrometer. The use of a grating divides the signal into several spectral channels. The parallel detection gives however rise to crosstalk between spectral channels leading to signal fading or SNR roll-off with depth. The advantage of SD-OCT is the acquisition of all the spectra at once, which could be faster than SS-OCT, but is limited by the CCD array velocity and the illumination time. A big advantage is that light sources of rather easy design can be used, which makes it potentially cheaper.

2.2.4 Swept source OCT (SS OCT)

A fast tunable laser is used, which sweeps a bandwidth $\Delta\lambda$ around a central wavelength. The common sweeping frequency is around 100 kHz. The different frequencies are separated in time, which makes it possible to record the spectral interference pattern over time and getting the depth structure with a single sweep. The spectrum is thus acquired with a single photo detector as a function of time and frequency. Swept source OCT is highly dependent on the laser properties: the laser must be fast enough (typically >100 kHz) to suppress motion artefacts due to involuntary motion of the sample. The difference between SD and SS OCT is the performance regarding SNR and resolution: due to less spectral crosstalk and the slower speed of CCD or CMOS cameras, SS OCT offers a better sensitivity and lower SNR roll-off with depth. A disadvantage is that faster swept sources together with the high-end data acquisition electronics are expensive.

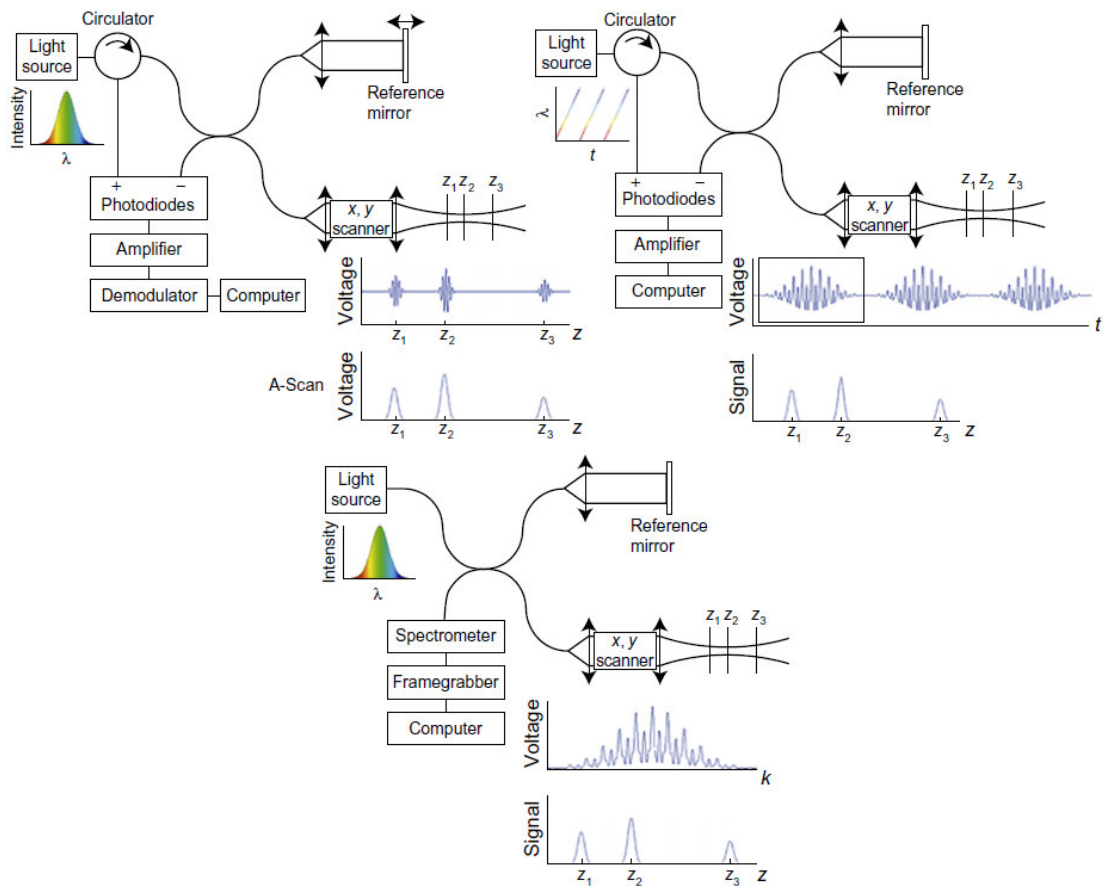


Figure 4, shows the schematics of TD-OCT using a broad bandwidth light source and scanning with the reference mirror, the schematics of an SS-OCT system using a swept source which scans through a set of frequencies and forms a time correlation to each frequency, as well as the schematic of an SD-OCT system which uses a broad bandwidth light source and a spectrometer to distinguish different frequencies. From [6]

Figure 4 shows a schematic of each setup. The OCT system used in this paper is a SS OCT system in Figure 4 right on the top.

2.3 Interferometer

The basic interferometer theory and OCT theory are adapted from [1] and [6].

A Michelson Morley interferometer is the basis of FD OCT systems. The interferometer is illuminated by a light wave, which is described by

$$E_i = s(k, \omega)e^{i(kz - \omega t)}$$

Equation 2, polychromatic plane wave.

$s(k, \omega)$ is the amplitude of the electric field, k is the wavenumber, ω the angular frequency, t is time and z is the optical axis coordinate. The beam splitter splits the power in two halves. For the reference path the reflectivity is around 1, the distance from beam splitter to mirror is z_R . For the sample arm the path length $r_s(z_s)$ is depth dependent, where z_s is the variable path length from the beam splitter. The sample path length is variable and continuous resulting from the varying refractive index $n(\lambda)$ of biological samples. To set an easy understandable example we define a number of delta reflections from the sample.

$$r_s(z_s) = \sum_{n=1}^N r_{sn} \delta(z_s - z_{sn})$$

Equation 3, series of sample delta functions.

The square of the electric field scales with the reflectivity $R_{S1} = |r_{S1}|^2$. To obtain the reflection as a function of the depth coordinate is the aim of OCT. The reflected sample beam can be described as,

$$E_S = \frac{E_i}{\sqrt{2}} (r_R \otimes e^{i2kz_R})$$

Equation 4, reflected beam for the sample.

The intensity of the interfered signal at the detector can be described as

$$I_D(k, \omega) = \frac{\rho}{2} \langle |E_R + E_S|^2 \rangle$$

Equation 5, Intensity of interfered signal.

where ρ is the responsivity of the detector and 2 is the factor due to the beam splitter. E_R and E_S are dependent on the temporal angular frequency, but can be eliminated by expanding the magnitude squared function.

This leaves the temporally invariant terms:

$$\begin{aligned} I_D(k) &= \frac{\rho}{4} [S(k)(R_R + R_{S1} + R_{S2} + \dots)] \\ &+ \frac{\rho}{4} \left[S(k) \sum_{n=1}^N \sqrt{R_R R_{Sn}} (e^{i2k(z_R - z_{Sn})} + e^{-i2k(z_R - z_{Sn})}) \right] \\ &+ \frac{\rho}{4} \left[S(k) \sum_{n \neq m=1}^N \sqrt{R_R R_{Sm}} (e^{i2k(z_R - z_{Sm})} + e^{-i2k(z_R - z_{Sm})}) \right] \end{aligned}$$

Equation 6, detector signal. From [1]

with the use of $S(k)$ being the spectral power of the light source. A Gaussian-shaped light source spectrum is used as $S(k)$ because it is nearly equal to the actual light shape frequently used in OCT and remains its simple Gaussian shape after FFT. The relation between the Gaussian function $S(k)$ and its inverse FFT $\gamma(z)$ being the degree of temporal coherence is given by

$$\gamma(z) = e^{-z^2 \Delta k^2} \leftrightarrow S(k) = \frac{1}{\Delta k \sqrt{\pi}} e^{-\left[\frac{(k-k_0)}{\Delta k}\right]^2}$$

Equation 7, Gaussian function of a light source spectrum.

The Fourier relation is called Wiener-Khintchin theorem. With k_0 being the central wavenumber and Δk the bandwidth at half width. This relation classifies the axial point-spread function (PSF), and its full-width at half maximum (FWHM) is called the coherence length l_c , the coherence length states the axial resolution as Eqn. 14 shows.

In SS-OCT, the signal is recorded sequentially in a single detector while the laser sweeps over the wavelengths. To get from wavenumber to the depth dependent structure information a Fourier transformation with the convention

$$\cos(kz_0) \leftrightarrow \frac{1}{2} \delta(z - z_0) + \frac{1}{2} \delta(z + z_0)$$

Equation 8, convention for Fourier transformation.

and convolution

$$f(z) \otimes g(z) \leftrightarrow F(k) * G(k)$$

Equation 9, convolution property of Fourier transformation.

is used.

The result of Equation 6 after using the conventions above and using Euler's rule, as well as shifting due to the delta function, the Fourier transform is performed. After FFT we obtain the so called "A-scan" containing depth information:

$$\begin{aligned} I_D(z) = & \frac{\rho}{8} [\gamma(z) * (R_R + R_{S1} + R_{S2} + \dots)] \quad \text{"DC Terms"} \\ & + \frac{\rho}{4} \left[\sum_{n=1}^N \sqrt{R_R R_{S_n}} (\gamma[2(z_R - z_{S_n})] + \gamma[-2(z_R - z_{S_n})]) \right] \\ & \quad \text{"Cross-correlation Terms"} \\ & + \frac{\rho}{4} \left[\sum_{n \neq m=1}^N \sqrt{R_{S_n} R_{S_m}} (\gamma[2(z_{S_n} - z_{S_m})] + \gamma[-2(z_{S_n} - z_{S_m})]) \right] \\ & \quad \text{"Auto-correlation Terms"} \end{aligned}$$

Equation 10, detector signal after delta shifting.

Equation 10 includes three distinct components:

- The "DC" term is the non-interferometric intensity term from the reference and sample reflections.
- The "cross-correlation" term is the interference term from the matching sample and reference beam. This term contains all the structural information of the sample structure.
- The "auto-correlation" term is the interference term, which occurs between two different reflections within the sample. This can be minimized by an increase of reference intensity, such that the auto-correlation terms are small compared to the non-interferometric background and the cross-correlation terms.

To explain the contribution of the different terms from Equation 10 we look at the A-scan signal obtained from a single reflector, which means that only DC and cross-correlation between sample and reference beam are present. The recorded spectrum has a cosine modulation with a specific frequency, which is inversely proportional to the path length difference between sample and reference reflection. With multiple reflectors we get a modulation of cosinoids with different frequencies as can be seen in Figure 5.

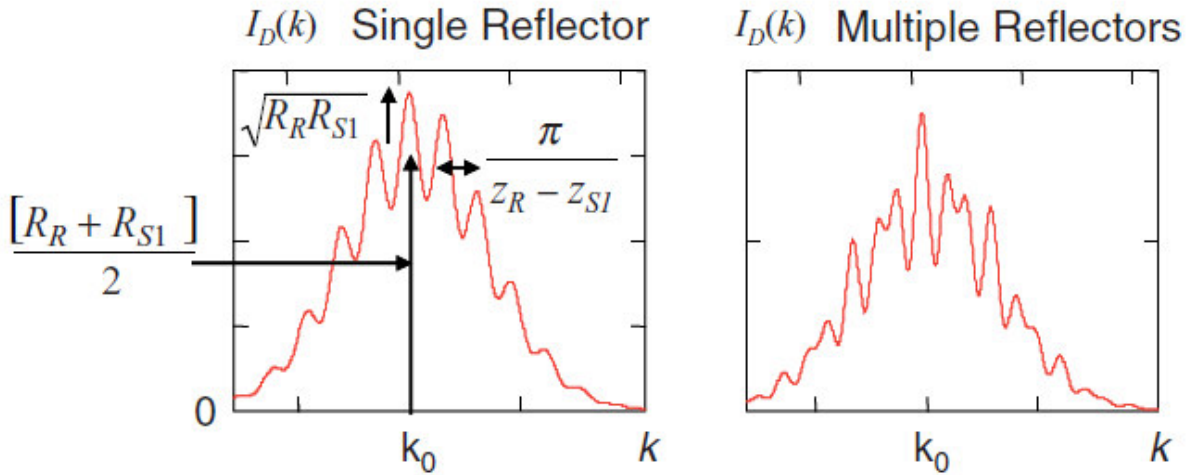


Figure 5, shows the interferometric signal for a single sample reflector forming a cosine structure of the interferometric signal (left). For more reflection in the sample we get a full modulation of cosine functions (right). The Amplitude of the left image is corresponds to the DC Amplitude, the small amplitude of the modulation to the cross-correlation amplitude. From [1]

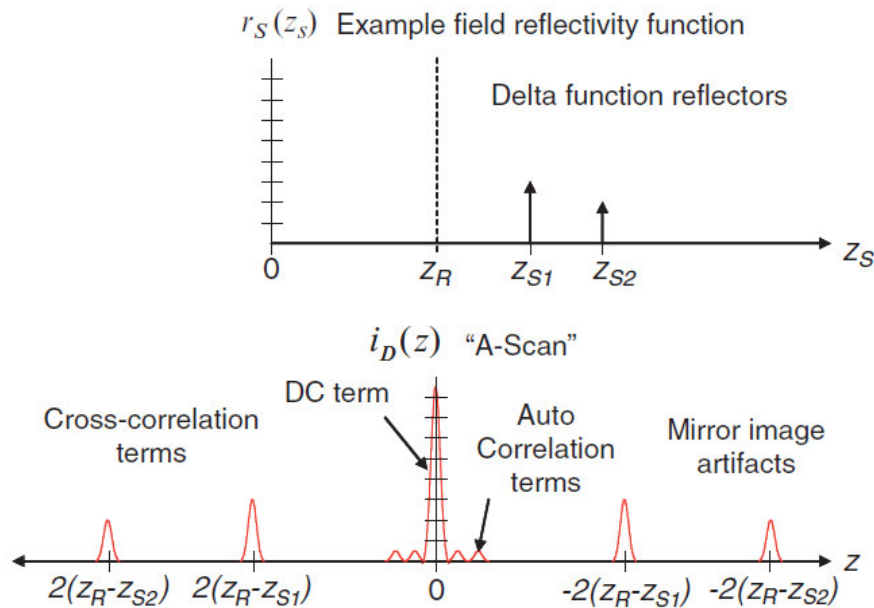


Figure 6, shows the different Terms which result from Eqn. 10, from two delta reflections from the sample tissue. From [1]

To demonstrate Eqn. 10 we look at a sample with two delta function reflectors, Figure 6 shows the DC Term, in the middle, the Auto correlation terms from the two delta reflections itself and then the Cross correlation terms from the two reflectors.

Equation 10 offers the z structure of the sample. As Figure 6 shows the DC term dominates the whole regime, but is rather easy to remove from the spectra by background subtraction. In Figure 7 the complex conjugated term of Eqn. 10 can be seen on the left side it contains the same information as the right images shows, thus it is removed in the image processing.

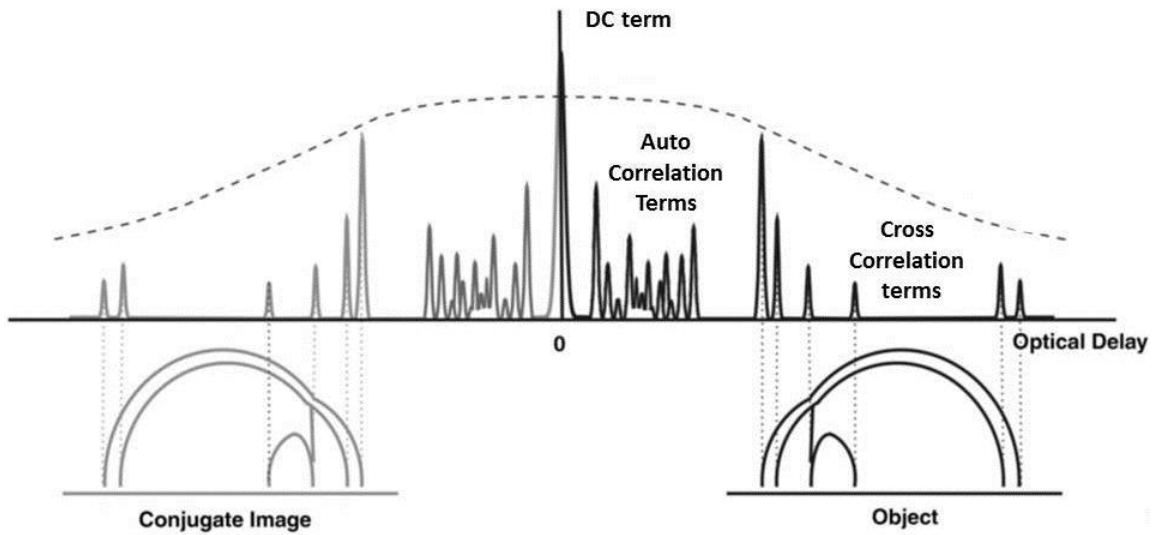


Figure 7, shows the signal which is detected at the photodetector, in the middle there is the DC-Term of the reference beam, the Autocorrelation term shows the self-interference of the backscattered light, and the cross correlation which contain the structural information. From [6]

2.4 Lateral resolution

The lateral resolution is dependent on the numerical aperture (NA) of the optical focusing path and the center wavelength (λ_0). Furthermore the optical system is cylindrically symmetric, which means only one lateral dimension needs to be described.

The lateral resolution gives the full width at half maximum power of the point-spread function.

$$\delta(x) = 0.37 * \frac{\lambda_0}{NA}$$

Equation 11, lateral resolution.

2.5 Axial resolution

The axial resolution defines the resolution in depth, which is proportional to the square of the center wavelength (λ_0) and inversely proportional to the Bandwidth ($\Delta\lambda$) of a Gaussian shaped light beam. Thus the axial resolution is inversely proportional to the power spectrum width.

$$l_c = \frac{2 \ln(2) \lambda_0^2}{\pi \Delta\lambda}$$

Equation 12, axial resolution.

l_c is the axial resolution of an SS-OCT system. As the bandwidth is inversely proportional to the axial resolution, a broadband light source is used to get a high axial resolution.

2.6 Image-SNR

To compare the used techniques in this work the signal-to-noise ratio difference between two images was determined. The image-SNR offers a way to compare different imaging techniques in its increase of SNR. SNR compares the power of the signal to the power of the background noise. As we want to compare two different images these images have to be compared in reference to each other.

The image-SNR is calculated according to [7]:

$$SNR = 10 * \log \left[\frac{\sum_0^{n_x-1} \sum_0^{n_y-1} [r(x, y)]^2}{\sum_0^{n_x-1} \sum_0^{n_y-1} [r(x, y) - t(x, y)]^2} \right]$$

Equation 13, Signal-to-noise ratio from reference to test image.

With r being the reference image and t the test image. n_x and n_y are image pixels in fast scanning and slow scanning direction, respectively. We compare the images vice versa; the difference in the image-SNR of both gives the total increase in SNR. In this thesis we used a process in the program imageJ to determine the SNR.

2.7 Doppler OCT

Doppler OCT is an aspect of OCT, which allows to determine the velocity of moving particles non-invasively. This allows measuring the blood flow for example in the eye, which is of great interest in many medical applications. The reconstructed intensity signal (A-scan) from the interferometer $S_{FDOCT}(z)$ is complex. It can be written in polar coordinates.

$$S_{FDOCT}(z) = |S_{FDOCT}(z)| * e^{i \cdot \varphi(z)}$$

Equation 14, Intensity and phase of the interferogram. From [8]

Where $e^{i \cdot \varphi(z)}$ describes the complex part with $\varphi(z)$ being the real valued phase spectrum and $|S(z)|$ is the amplitude spectrum. Compare now two A-scans at the same position with a time difference $\Delta\tau$. If the particles of a distinct position do not move, there will be no phase difference $\Delta\varphi(z)$. In case they are moving this phase difference allows determining the velocity of these particles by the following relation:

$$v(z) = \frac{\Delta\varphi(z, \Delta\tau)\lambda_0}{4\pi\Delta\tau n}$$

Equation 15, velocity of particles in z direction. From [8]

where $v(z)$ is the velocity measured in axial z-direction, $\Delta\tau$ is the time difference, $\Delta\varphi$ the phase difference between 2 A-scans, n is the refractive index of blood and λ_0 the central wavelength. Furthermore, if we determine the moving particles as blood cells, they will move in a distinct direction. To determine now the exact velocity, the angle of these blood vessels with respect to the sample beam has to be known. The absolute velocity can be calculated by

$$v_{abs}(z) = \frac{v(z)}{\cos(\alpha)}$$

Equation 16, absolute velocity. From [8]

The angle α is the angle between the incoming beam and the blood vessel. It's of importance to know the Doppler angle α exactly to calculate the velocity with a normal single beam system, furthermore we get a problem at angles close to 90° , as the velocity tends to infinity. To avoid the exact measurement of the angle it is possible to calculate the absolute blood flow directly from the

en face cross section of the vessel [9], this calculation uses the effect, that the dependence of the velocity on $\cos(\alpha)$ due to the en face plane cancel each other. The only problem occurs at rather small angles, where the en face plane is rather difficult to measure correctly.

A second way to eliminate the dependency on the Doppler angle is the use of a second beam. Dual beam bidirectional OCT has two different beams with a distinct angle $\Delta\alpha$. Focused onto one point in the sample, the unknown Doppler angle α can be eliminated as just the angle between these two beams needs to be known. Although the Doppler angle is eliminated, a dual beam system is still dependent on the angle $\Delta\beta$ between the illumination plane and the vessel flow direction:

$$v = \frac{\Delta\Phi}{2 * nk\tau * \cos(\Delta\beta) * \Delta\alpha}$$

Equation 17, angle independent dual beam velocity. From [10]

Dual beam Doppler OCT allows calculating the velocity even for small angles. Thus in the setup used in this paper a dual beam bidirectional OCT has been used. To again avoid the dependency of the en face angle another method can be used as demonstrated in [10]. Using a dual beam system with an additional rotation of these two beams can guarantee to keep a small $\Delta\beta$ ($<25^\circ$). To rotate the two beams a Dove prism in combination with an electro motor was used. This allows rotating the two beams twice during one rotation of the dove prism. For the determination of the blood flow now a good selection of each vessel needs to be done. The vessel can be selected as they have a similar phase shift due to the velocity of the blood flow. For this section the mean velocity is calculated and multiplied with the vessel surface, which gives us the total blood flow:

$$F(t) = \int_A \vec{v}(t) \vec{dA} = \int_A \vec{v}(t) \vec{n} dA.$$

Equation 18, total blood flow. From [9]

with dA being the element of surface and \vec{n} its normal surface.

Figure 7 shows the different angles from the two incoming beams and a blood vessel and its flow direction.

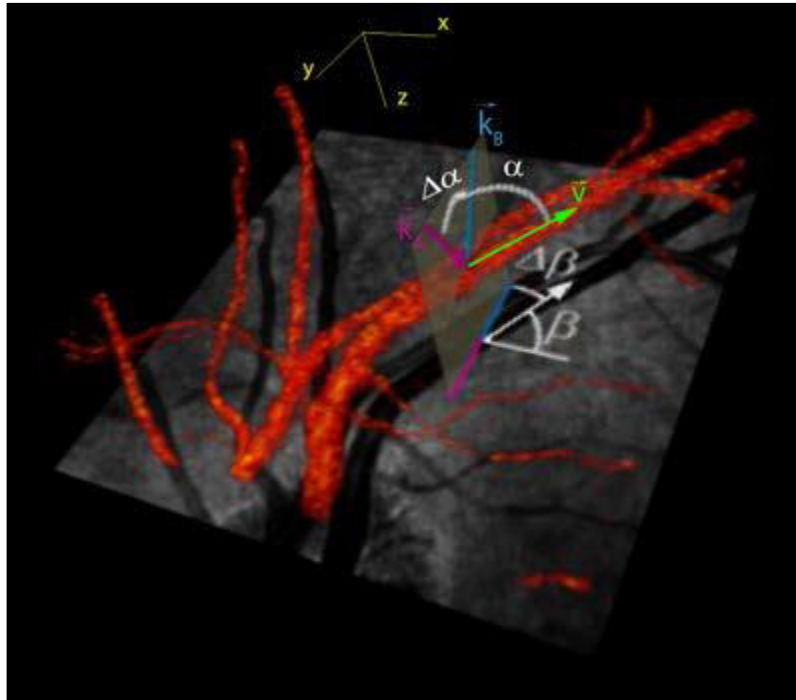


Figure 8, shows the Doppler angle α between the laser beam and the blood vessels as well as the angle between the two beams k_A and k_B $\Delta\alpha$. In the fundus projection, the vessels have an angle β and the plane of the two beams an angle $\Delta\beta$ to the scanning coordinates. From [91]

2.8 Angiography

Angiography is the medical imaging technique to visualize blood vessels and organs in an organic sample. State-of-the-art technique for performing ocular vascular imaging is angiography using fluorescein (FA) or indocyanin green (ICGA) as contrast agents. Normally these agents are injected in an antecubital vein, with enough speed to have a fast distribution. Flashing now the eye with blue light induces fluorescence of these contrast agents, which is detected with a camera. The drawback of FA/ICGA is its time-consuming (up to 30min) and invasive character, requiring the intravenous application of contrast agents. Eventual side effects include allergic shock, nausea, vomiting or multiple painful needle sticks. This prohibits repeated examinations of patients or the screening of large populations, which would be advantageous for early detection of vascular related diseases. Moreover, these techniques cannot provide depth information and are limited by the two-dimensional (2D) nature of the images. OCT angiography has the potential to provide vascular contrast in a depth resolving manner, with high resolution, and without the need of FA/ICGA administration. OCT angiography may be used to diagnose diseases related to ocular vascularization like glaucoma, diabetic retinopathy, and age-related macular degeneration (AMD), which are the leading causes of blindness in the industrialized world. The combination of both, D-OCT and OCT angiography therefore offers important biomarkers for disease diagnosis that are currently not available, mainly due to technological reasons.

OCT Angiography can be performed via speckle and phase changes between two successive B-scans (Scan at one lateral position). Speckle is an interference phenomenon, which is visible by interfering coherent light with random phases. Speckles are affected by sample properties like structure and motion as well as by the properties of the light source and the used optics in the sample path. Speckles are the result of superposition of many random wavelets. Statistical properties of the laser speckle can be described by the amplitude and phase of these wavelets, which are statistically distributed and have phase uniformity. The intensity of the backscattered sample light has different intensity over time and depends on this intensity and the detector itself, which leads to a Rayleigh distribution for the speckle. Speckle can be used as an information carrier, as speckle is sensitive for motion. While in static structure the speckle fluctuates just like noise the speckles change during motion. Due to the speckle change it is possible to determine whether there is motion or not. The method used is called speckle variance OCT (SV-OCT), this allows to

identify microvasculature by calculating the intensity variance between two or more tomograms at the same transverse position. Contrast is based on the speckle variance between blood flow and static structure. Speckle variance is calculated based on the log-intensity tomograms:

$$I(x, y, z) = 20 * \log[|FFT(I(x, y, k))|]$$

Equation 19, Interferogram, logarithmically scaled. From [11]

where k is the wavenumber, which gets transformed via the FFT to the depth coordinate z , $I(x, y, z)$ are the tomograms and (x, y, z) are fast, slow scanning and depth coordinate. The squared intensity speckle difference between successive Tomograms is written as

$$D(x, y_i, z) = [I(x, y_{i+1}, z) - I(x, y_i, z)]^2$$

Equation 20, Speckle variance. From [11]

where i is the number of tomograms taken at the same vertical position (in our case 4). Which means we acquire 4 full B-scans within 20 μ s at the same position.

Furthermore a threshold T is set to choose only these differences ($M(y)$) which are below this threshold:

$$M(y) = \sum_{i=0}^{N-1} \left(\left[\sum_{x,z} D(x, y_i, z) \right] < T \right)$$

Equation 21, Thresholding. From [11]

This should discriminate these speckle variances which are rather high due to sample movement or scanner position change. Without proper thresholding these variances would dominate the variance image and destroy the speckle variance profile of the other B-scans. The vascular contrast $V(x, y, z)$ is obtained by averaging only over the remaining M :

$$V(x, y, z) = \frac{1}{M(y)} \sum_{i=0}^{N-1} \left(\left[\sum_{x,z} D(x, y_i, z) \right] < T \right) * D(x, y_i, z)$$

Equation 22, Summation of speckle variance. From [11]

This method from [11] is more robust against motion artifacts, than a variance analysis over the full tomogram series acquired at the same position, thus images with strong variance due to movement gets rejected.

2.9 The human eye

The human eye is one of the most important organs in the human body, it enables fast interaction with the environment. It consists of three different layers, the first layer consists of the sclera and the cornea. The middle layer holds the choroid, ciliary body and the iris. The deepest layer is the retina. All these components are important for the formation of a clear image on the retina. The iris acts like a diaphragm, which regulates the amount of light, which is entering the eye. The ciliary body contains muscles which can be contracted, this influences the refractive power of the lens. The retina is responsible for the transformation of optical light into electrical signals.

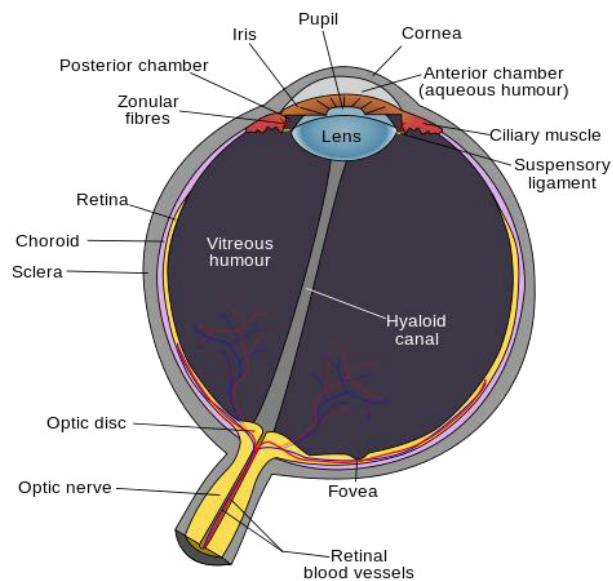


Figure 9, shows the internal structure of a human eye, The Cornea and the Sclera form the outer Part of the eye, the Iris, choroid and ciliary body the second layer and the retina the innermost layer, which holds the photoreceptors. From [12]

2.10 The retina

The retina is the most important part of the eye, it contains the photosensitive cells, the rods and the cones. Two characteristic parts of the retina are the optical nerve head and the fovea.

Responsible for sharp vision is the fovea. The fovea has the highest density of cones but has actually less rods, therefore it's less sensitive to light. These cells are responsible for the vision, rods are photoreceptors which guarantee our dark or scotopic vision. The cones are responsible for the color vision. The outer layer contains the cell bodies of the photoreceptors. These cells convert the light energy into electrical signals, which are transferred via the optic nerve head (ONH) to the brain. The optic nerve is the region where the vessels enter and exit the retina. At the ONH are no cones or rods, due to the vessels, which enters the eye.

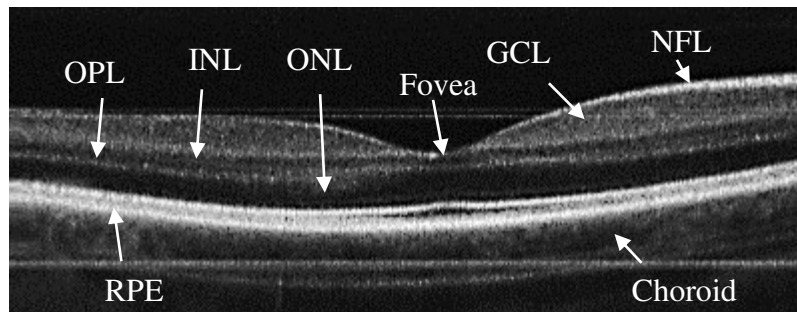


Figure 10, shows the detailed structure of the Retina at the Fovea

In Figure 10 the different layers of the retina are labeled according to [13]. Starting with the nerve fiber layer (NFL), this layer contains the ganglionic axons which travel towards the optic nerve head from the fovea where the NFL is rather thin. It becomes thicker towards the ONH, because the ganglion axon fibers run all towards the ONH. The ganglion cell layer (GCL) contains about 1.2 million ganglion cells, amacrine cells, astrocytes, endothelial cells and pericytes [13]. The thickness of the GCL is around 60-80 μm .

The inner nuclear layer (INL) consists of 5 different types of cells, the horizontal, bipolar, amacrine, interplexiform and the Müller cells. In the outer plexiform layer (OPL) the photoreceptor cells are connected to the bipolar and horizontal cells of the INL. The outer nuclear layer (ONL) holds the photoreceptors and is thickest at the fovea. The retinal pigment epithelium (RPE) holds around 3.5 million RPE cells together. This layer has the strongest reflection in OCT. The last part is the choroid, which supplies the inner retina with blood. The choroid receives 80% of the ocular blood flow.

Most eye diseases affect the retina and have an impact on blood flow or structure of the retina, thus it is of importance to acquire information about the retinal structure and microvascular network. In order to get this structural information of the eye laser light in the near infrared spectrum is used. The absorption of water is rather low at infrared and it's possible to enter several mm into a biological sample. The used center wavelength in this thesis is 1050nm.

Figure 11 shows how thick the NFL gets towards the ONH and also shows where the photoreceptors are held in the RPE. At the ONH all vessels and nerves enter the eye.

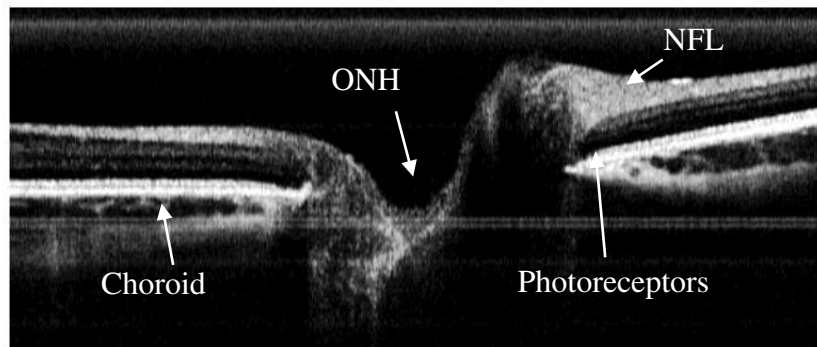


Figure 11, shows the detailed structure of the Retina around the ONH. Self-generated

2.11 Remapping

In FD-OCT depth structure is reconstructed from the different wavelengths. This is done by using the FFT which transfers the wavenumber k to the depth position z . A problem might occur as the spectra might not be evenly spaced in k . For a good depth profile an evenly spaced spectra in k is necessary to relate the depth coordinate correctly to a specific wavelength. As this might not be the case a remapping of the spectra has to be considered. Without this remapping a depth dependent broadening of the coherence peak occur, which is similar to dispersion mismatch (Fig.12). SSOCT allows the detection of the spectra linear in k by hardware- k -triggering, or sweep phase control. In our system the synchronous k -trigger trace can be saved separately and used for proper mapping in post processing. But in our case we apply the Hilbert transformation to the reference interference pattern, measured with a single reflector in the sample arm for this remapping. The Hilbert transform allows to generate the phase signal of the recorded interference pattern. Then one selects a spectral interval, where the phase change is close to linear. This section is used to remap the spectra to get even spaced spectra in k , which enabled to recover the axial resolution.

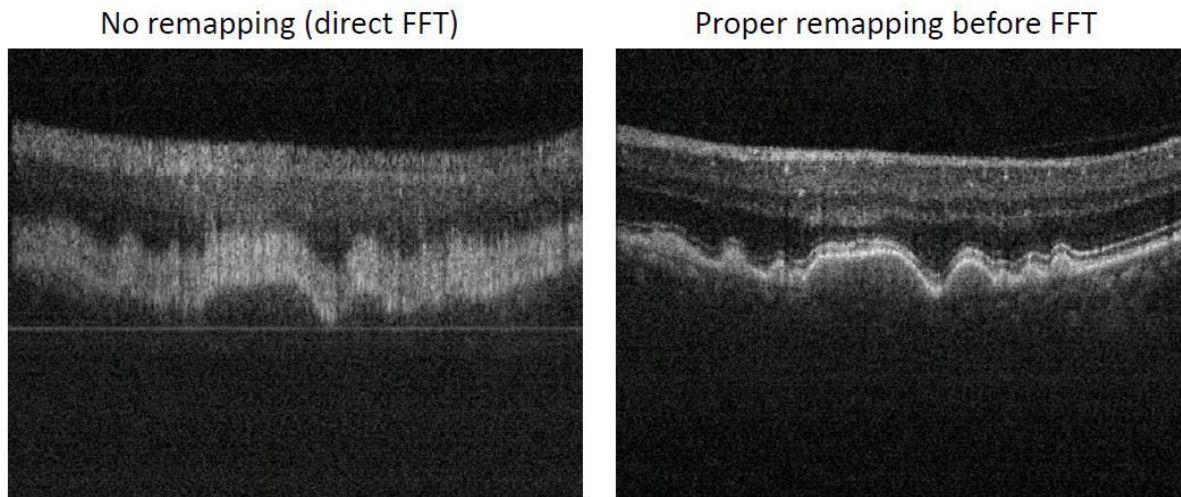


Figure 12, shows the result of no proper remapping, a broadening of the depth structure is visible which destroys the exact depth position. From [14]

2.12 Errors

There are several different errors which can occur in an optical system during scanning a biological sample. The most important are mentioned below.

2.12.1 Dispersion

Dispersion occurs in the optical path, and needs to be carefully balanced in an interferometer system. Otherwise different wavelengths experience different optical paths, which leads to degradation of the depth resolution and reduces sensitivity. Phase shift and change of the mean wavelength are less important, but accrue as well. The easiest way to realize dispersion compensation, is implementing additional dispersion material in the reference arm, matching the dispersion in the sample arm.

Normally dispersion balancing is done by using a prism pair that allows to adjust variable thickness of BK7 material. This is a flexible method to compensate dispersion.

Dispersion compensation can also be done in post processing, but it is time-consuming and an effort which can be easily skipped by implementing dispersion material properly.

2.12.2 Crosstalk

Crosstalk is an error which can occur in a multi-channel transmission system, when signal from one channel influences another channel. In our dual beam system crosstalk can occur between the two beams, when backscattered light from beam 1 interferes with the reference arm of beam 2. This can be easily prevented by using different path lengths.

2.12.3 Motion artifacts

As OCT scanning needs time, motion of the sample during the measurement causes SNR reduction and image degradation. This is the reason, why OCT-systems should have a short measurement time and a stable setup. Motion can occur in lateral and axial direction, where the lateral motion changes the position of the beam in the eye, axial motion reduces the SNR as the focus gets shifted. This motion is also called bulk motion. Cross-correlation techniques in post-processing help to reduce those motion distortions.

3 METHODOLOGY

3.1 System Setup

The OCT setup used in this work is the same as described in [10]. It is a dual beam Doppler OCT device employing a swept source operating at 1050nm center wavelength. Figure 13 shows the optical setup. The swept source used is a multiplex source by Axsun (A1300467) with an A-scan (one sweep) frequency of 200 kHz. This source has a bandwidth of 105.62 nm resulting in an axial resolution of around 5 μm in air.

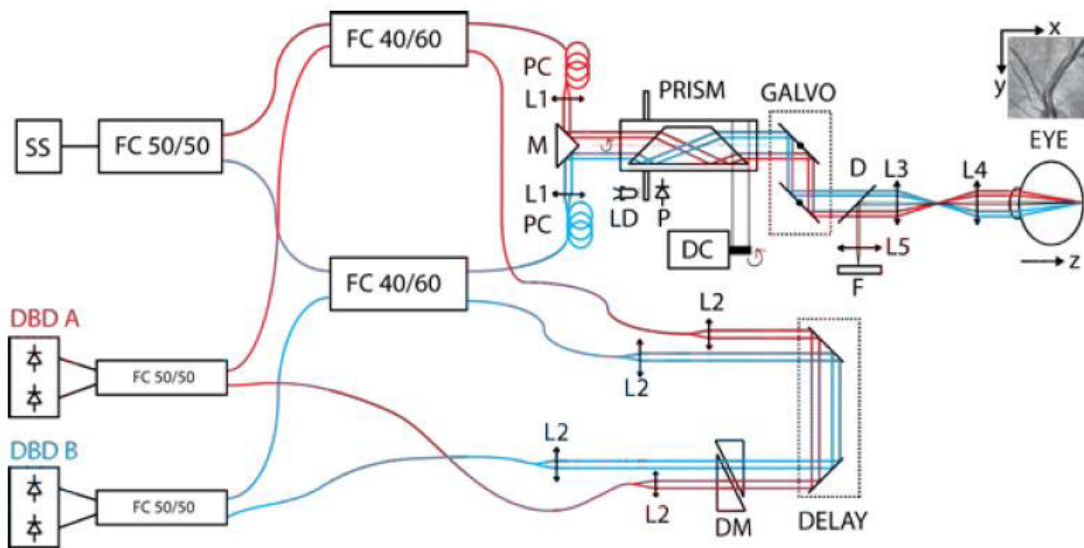


Figure 13, shows the schematic of the OCT-Setup. The red and blue line characterizing A and B beam. From [10]

The light from the swept source is split into two beams by a 50/50 fiber coupler (FC). After this it is again split by a 40/60 FC, which means 60% and 40% for the reference and sample arm respectively. The sample beam passes through a Dove prism, which enables to rotate the beam by 360°. This enables to measure blood flow angle independently. After this prism it is projected to a galvo scanner, which scans over a maximum of 16° field of view (FOV) horizontally and vertically. The reflected beam from the eye interferes with the reference beam on its way back to the detector (EBR37000x-01, Exalos). The reference arm is axially moveable to match the coherence window with the sample arm, furthermore it contains dispersion compensating glass prisms. To minimize crosstalk the path lengths of beam 1 and 2 are different. The interference is measured with a dual-balanced detector (DBD). The signal is

digitalized at 250MSamples/s with a 12bit analog-to-digital converter (ATS9350, Alazartech). The data is saved on an SSD hard drive which enables fast saving due to its fast memory access. The data is stored in OCT files which consist of the binary spectral information in 12 Bit, and a header with information on the scanning angle, the remapping, and other notations as ID number or left or right eye. The total power for each beam at the cornea is $\sim 1.2\text{mW}$, which is consistent with the ANSI standards safe exposure limits, leading to a measured sensitivity of $\sim 94\text{dB}$. The telescope (L3, L4) in the sample arm has an angular magnification of 1.5x. With a beam size of $\sim 1.3\text{mm}$ at the cornea, the theoretical spot size on the retina is $25\mu\text{m}$. The signal processing is done in LabVIEW. The post processing, which is motion correction, flattening, and speckle variance calculation was programmed in MatLab.

3.2 Multiplexed Laser Source

The first Step of this work was to integrate a new swept source from Axsun (A1300467) to an existing dual beam Doppler OCT device. This multiplex swept source consists of actually two lasers, which sweep alternately. When the sweep of the first laser is done, the back sweep gets suppressed and the forward sweep of the second laser continues. This offers a series of up sweeps with close to 100% duty cycle, which allows doubling the frequency from originally 100 to 200 kHz. Each sweep operates with a duty cycle of around 45%. The central wavelength of this swept source is still 1050 nm, which is in the near infrared, and the sweeping broad bandwidth is 105.62 nm. This results in an axial resolution in air of 5 μm as for the individual sources.

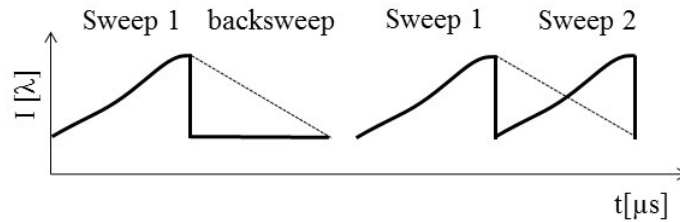


Figure 14, shows the sweep structure of the new Axsun Laser. Self-generated

Figure 14 shows the sweep structure and the performance of the multiplex laser. The first curve shows the timing of the single source: after the first sweep, the back sweep is suppressed, resulting in the duty cycle of less than 50%. The second curve shows the improved duty cycle by interleaving two sources: during the suppressed back-sweep of the first source the second source jumps in. Due to the fact that the sweeps origin from two different lasers the remapping of each sweep has to be calculated separately, as there is no guarantee for a same or similar spacing of the wavelength in k . Each sweep gets remapped separately by using the Hilbert transformation and selecting a linear section of the phase. The signal is then rescaled to 2000 spectral sampling points. After the remapping to linear k space the FFT needs to be applied to get from the spectral domain to the space domain, being the actual reflectivity profile in depth or A-scan. We now have 2 images from each sweep, which can be interleaved in post-processing. This enables an exact remapping for each sweep and allows to exploit the advantage of doubling the lateral sampling due to changing from 100kHz to 200kHz A-scan rate. In **chapter 4** we present results that confirm the improved imaging performance with the faster laser source.

3.3 High Speed Galvo Scanner

High speed galvo scanners were integrated into the setup to gain scanning speed and improve the field of view. The original scanners introduced already strong jitter when increasing the amplitude to cover a 16° FOV. The new scanners by Cambridge Technology (6215HM60) should guarantee a FOV of 30° with the same scanning frequency, which is expected to improve current OCT angiography capabilities.

During implementation of the new scanners the reference path of our system was further optimized. After implementing the new scanner the wavelength calibration, which means the remapping procedure has to be performed again, due to slight changes in the sample arm path as well as the optimization of the reference arm. The performance of improved setup has then again been benchmarked against the original setup and the results are presented in **chapter 4**.

3.4 Spectral Splitting

OCT angiography requires dense sampling in order to maintain good vascular contrast. This limits systems operating at 100kHz to a maximum field of view of 8° , which is much less than the gold standard of fluorescein angiography covering 20° and more. Stitching of smaller FOV patches is possible, but requires a good fixation of the patient, with a proper control of the measurement region. This is only possible in combination with a retinal tracking system. Another less complex solution is to increase the system speed. Doubling the FOV means that we need to increase the A-scan rate by a factor of 4 as we increase the scanning area. Employing the multiplex laser already accounts for a factor of two. In the present work a technique called split spectra method was implemented to virtually gain further acquisition speed and spatial sampling, while maintaining the same measurement time. The latter is critical in case of in-vivo measurements, as involuntary motion might destroy the comprehensive. This method splits the recorded spectra into two sub spectra of half the optical frequencies. Using continuous lateral scanning in fast axis direction enables an effectively increased sampling by a factor of two. This is due to the fact that the spectra are recorded over time: after half of the spectrum is swept the scanner is located already at another lateral position where the other half of the spectrum is recorded. This allows increasing the field of view in SSOCT while keeping the same transverse sampling and measurement time.

The full spectra is sampled by 2432 points covering 105.62 nm. The splitting results in two sub-spectra with a bandwidth of 52.81 nm each which decrease the axial resolution according to Eqn. (17) to $10 \mu\text{m}$. After splitting the sub-spectra are further weighted by a Hanning window to avoid increased noise after FFT due to edge effects.

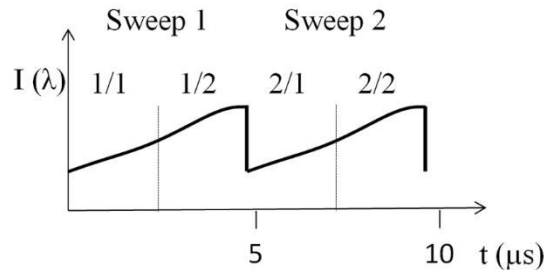


Figure 15, shows the split spectra approach.
Self-generated

Compared to the 100 kHz standard OCT device we have now a fourfold increase in lateral sampling which indeed allows us to cover 16° instead of 8° FOV without losing resolution and contrast performance. We have 2 spectra from each sweep of the multiplex laser and both spectra are further split into two halves resulting in 4 individual spectra that need to be processed individually. After FFT of the spectral data, we obtain 4 different tomograms that can be appropriately interleaved in order to obtain the full tomogram with four fold sampling. For this interleave there might be a change in intensity and a slight shift in axial structure resulting from the different mapping procedures and the different center wavelengths of each half-spectrum. Afterwards the image intensity is squared, changed to logarithmic scale, and saved as unsigned 16bit TIF files. This is done by dividing the whole image through the maximum value and then multiplying it with 2¹⁶. The tomograms read

$$I(x, y, z) = 20 \cdot \log[|FFT(I(x, y, k))|]$$

Equation 23, Tomograms logarithmically scaled. Self-generated

with (x, y, z) being the respective fast scanning, slow scanning, and depth coordinate. To calculate the angiography the speckle variance method described above in **chapter 2** is used. The splitting is reducing the axial resolution by half (from 5 to 10μm), but offers an improve in image SNR of OCT angiography images by relaxing the sensitivity to bulk motion noise in axial direction. In **chapter 4** we demonstrate the performance in-vivo at different locations of the human retina and verify the improvement in image SNR quantitatively. Another way to increase contrast is not using the split spectra to enhance the field of view but instead averaging these two images to increase SNR, as was demonstrated in [15].

3.5 Bulk motion compensation

As in-vivo measurements of the human retina are usually affected by involuntary motion. It is therefore of great importance, that a proper compensation of resulting axial displacement between successive tomograms is done. There are several different post processing techniques, which can be used in our case we used the motion compensation over cross correlation.

For each B-scan a section of A-scans was selected and the cross correlation between successive B-scans was determined. The cross correlation measures the similarity of two arrays and determines the difference. With this difference in pixel a shift algorithm can be applied for each following B-scan. Another form to find this difference is the algorithm “finddelay” in Matlab, which produces already the value for the bulk motion.

If the shift between successive B-scans is found a circular shift with the following B-scan in reference to the first one can be done. This reduces the axial bulk motion. Although it is not perfect it's a good way to reduce such motion.

3.6 Angular compounding

As the system is a dual beam system the angle of 3.9° between these two illumination beams gives rise to different speckle patterns in the respective recording planes. Adding the final images of both channels leads to speckle averaging and is called angular compounding. In general dual beam systems suffer from intensity reduction for each channel, since laser safety standards restrict the amount of light entering the eye. Thus, the sensitivity of each channel is lower than that of a single beam system. Still, dual beam systems have the distinct advantage of enabling to measure angle independent blood flow within tissue. However, if only structure tomograms are of interest, as well as for OCT angiography, using only the information of a single channel comes at the price of lower sensitivity. To overcome this intensity reduction angular compounding was introduced. Having two channels available with distinct illumination directions allows for combining the both images and thus mitigating the loss in intensity. To combine the images from each channel, the fundus projections of both angular channels need to be co-registered using an appropriate elastic registration algorithm. In our case the JUnwrap plugin of the open source image processing software “ImageJ” [16] does the job. Our aim was to apply the angular compounding technique to OCT angiography images of both angular channels. For the angiography projections we calculated maximum intensity projection over around 10 en-face depth slices from the motion contrast volumes obtained by the technique explained in **chapter 2**. The plugin JUnwrap constructs a transformation Matrix, which transforms and registers one image elastic and consistent to the second image, that serves as reference. After co-registration, these two pictures are summed which averages speckle and thereby increases contrast. Ultimately, this increases the image SNR compared to using just a single beam. The results are demonstrated in **chapter 4**.

3.7 *Flattening of the Tomogram*

The retina of a human eye has a curved form as the eye is a spherical object. For medicals the en face projection of the retina is of importance as they are used to look at 2D fundus images or 2D the fluorescence angiograms. OCT tomograms offer a full 3d view of the retina that allows extracting also en-face views. As the human retina is spherical a normal en-face cut doesn't offer a proper vision of just one layer. It is getting mixed due to its spherical form. A way to compensate for this curvature needs to be found. We implemented a flattening processing which converts the curvature to a static depth position. This compensation is done by finding the maximum intensity position of the RPE over one whole B-scan. After finding this maximum position a low order polynomial fitting is done. Each A-scan of the B-scan can then be shifted by the local difference between the polynomial fitting curve and the constant depth position. This post processing was a good solution for fovea images, at the ONH it is difficult to overcome the RPE gap at the lamina cribrosa region.

3.8 *In Vivo Measurement Protocol*

To demonstrate the feasibility of the split spectrum and the angular compounding method for increasing the sampling density, we compare 8° and 16° patches acquired at 400 kHz (multiplexed laser, spectral splitting) to patches acquired at 100 kHz (single sweep laser, full spectrum) at the fovea region and optic nerve head (ONH) of a healthy volunteer. The x- scanner (fast axis) scans linearly whereas the y- scanner (slow axis) scans in steps with a vertical sampling of 400 steps. For OCT angiography we record N=4 tomograms at each sampling point in y- direction resulting in a total of 1600 tomograms per volume. The lateral number of sampling points is 200 for 100 kHz acquisition, 400 for 200 kHz, and 800 for the split spectrum method at 400 kHz. The total acquisition time is 7.8 sec for all cases. The presented in-vivo measurements were in accordance with the local ethics committee regulations and the declaration of Helsinki.

4 RESULTS

In the following section the results obtained with the mentioned system modifications will be presented and compared to those obtained with the original setup.

4.1 Multiplexed Laser

As explained in **chapter 3** employing a multiplexed Axsun laser (A1300467) offers an increase to 200 kHz in sweeping frequency, which results in the possibility to sample twice as many points in fast scanning direction within the same time as with the former used 100 kHz source. The samples were taken from a healthy volunteer over a field of view (FOV) of 8° across the fovea centralis. After applying the speckle variance calculation introduced in **chapter 2** the obtained angiograms were compared.

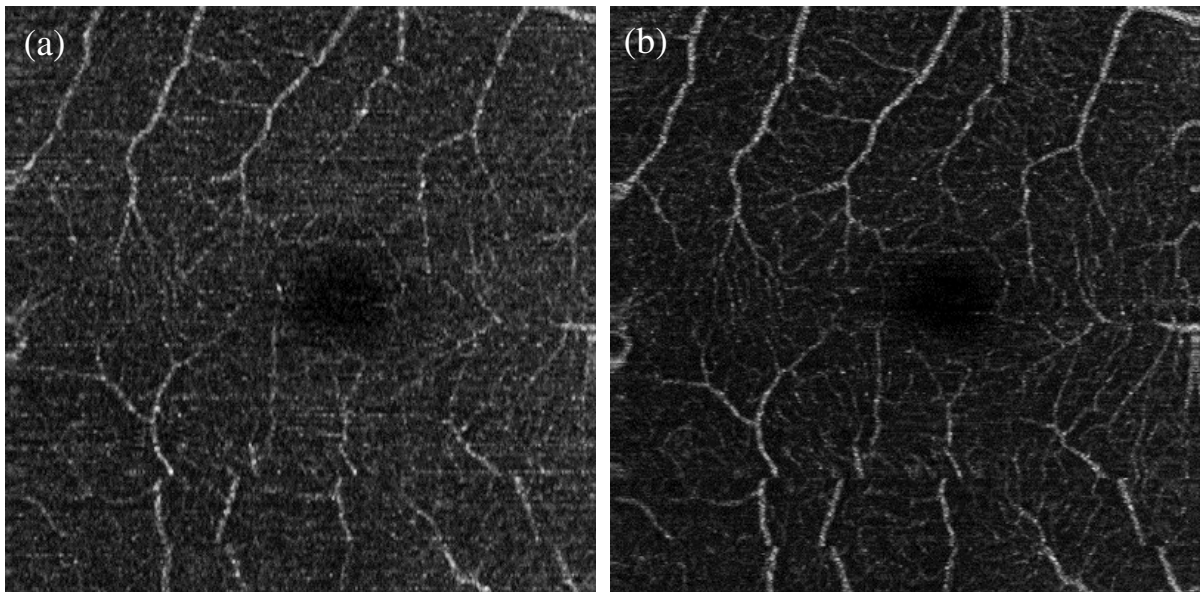


Figure 16, shows the 8° section around the fovea with 100 kHz on the left side and in comparison the 8° section of the fovea with 200 kHz. Self-generated
Figure 16 (b) shows an increase in image SNR of 2,54 dB compared to 16 (a) as calculated with the SNR formulae Eqn. 13. Also much more details of the small capillary bed are visible in 16 (b) as the noise is reduced. Doubling the samples in the fast scanning, or x direction is a good solution to improve the contrast. The ultimate limitation is of course the physical lateral resolution. In theory an oversampling factor of two is the minimum and higher oversampling helps to increase the contrast.

4.2 High Speed Galvo Scanner

The new galvo scanner pair by Cambridge Technology runs more stable at higher frequencies above 100Hz resulting in less vibration and higher phase stability. Further improvement of dispersion matching in reference and sample arm and of the remapping procedure helped to improve the quality of the images, and to cover a larger field of view.

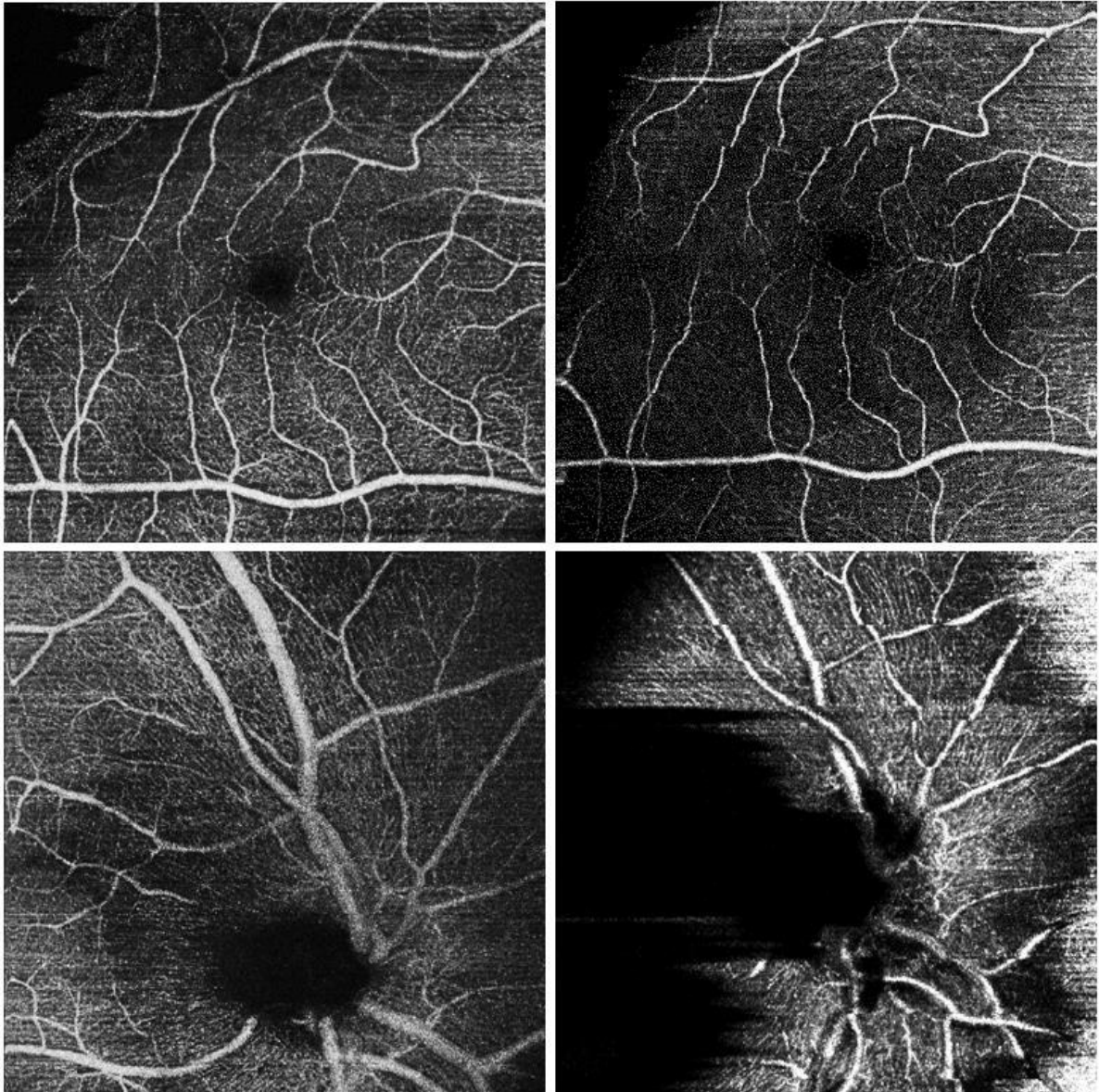


Figure 17, shows the new images made with the Cambridge scanner in comparison with the old ones with the Thorlabs scanner. On the left side are the new images with 16° at the Fovea and the ONH. On the right side are the images with the old scanner at nearly the same position. As can be seen with the new scanner more structural details are visible.

Figure 17 shows the fovea centralis and the ONH with 16° FOV. The right column of Fig 17 displays the angiographies of the respective retinal regions as obtained with the previous scanner system. Black areas in the lower right image are a result of improper axial registration of the B-scans. Images of the left column are obtained with the high speed scanning system as well as with the improved resampling procedure. The improved level of details with the optimized system is well visible within the indicated region of interest in the lower row.

4.3 Spectral Splitting

As mentioned the split spectra approach was compared to standard signal processing on data obtained with 200 kHz and 100 kHz A-scan rate. The split spectrum processing was applied to the data obtained with 200kHz. First we compared the three methods described above applied to in-vivo data taken at the same region of the fovea. The second step consisted in comparing the performance on images with doubled FOV.

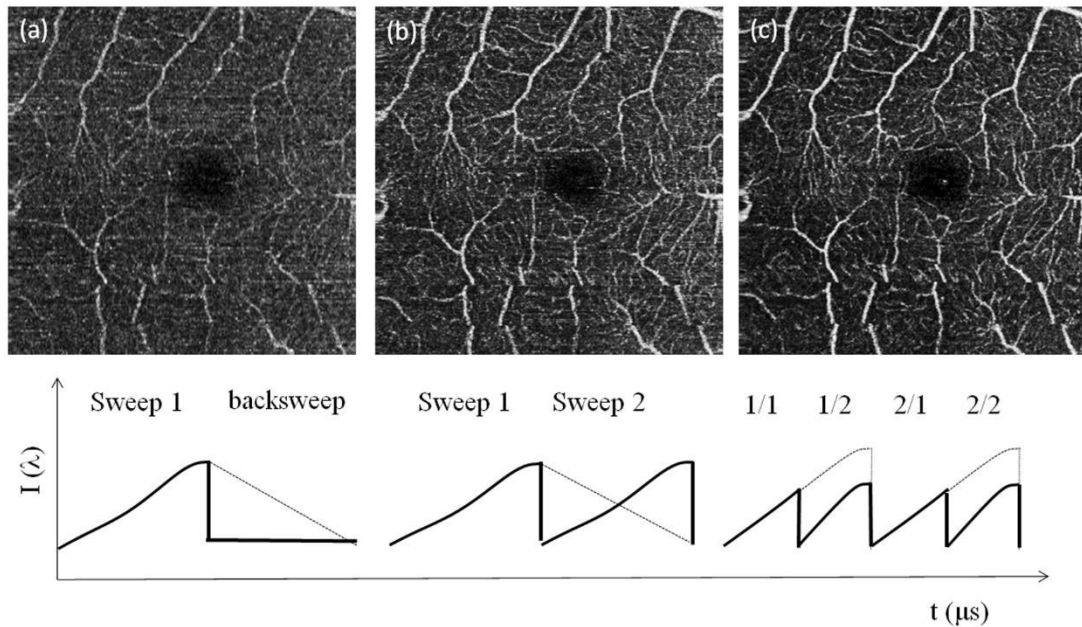


Figure 18, (a) shows an 8° section around the Fovea with a standard 100 kHz system, (b) shows the result with the new multiplex laser working at 200 kHz and (c) shows the same area with the multiplex split spectra reaching virtual 400 kHz. Self-generated

Fig. 18 (a) shows an example of OCT angiography of the parafoveal region with single sweep acquisition at 100 kHz and conventional processing obtained. The FOV was 2.3mm x 2.3mm corresponding to a scanning angle of 8° in both directions. The 2D angiograms are calculated as maximum intensity

projections across a selected depth range from the motion contrast volumes. In order to enable assessment of vascular structures at equal depth we flattened the motion contrast tomograms with respect to the highly reflective inner-outer photoreceptor segment boundary. Furthermore, we registered the intensity tomograms axially prior to motion contrast analysis. The respective sweep structure is depicted underneath the angiography in Figure 3. A comparison with the multiplexed sweep acquisition in Fig. 18 (b) and with images obtained after applying the split spectrum approach demonstrates the improvement in sampling rate and thus image quality. Whereas in Figure 18 (a) details of microvasculature are revealed only fragmentary, most of the small vessels are fully visible in Figure 18 (b). The split spectrum approach improves then further the signal to noise level in the angiographies, which was already demonstrated in [11] by introducing the image signal to noise value **Equation 13**. For the 8° Fovea section we calculated an improvement of 2,26 dB in SNR for Fig. 18(c) as compared to Fig. 18(b).

The increase of total sampling points by a factor of 4 allows increasing the FOV from 8° to 16° in both, x- and y- direction without sacrificing sampling density and measurement time. Fig. 19 (a) shows an 8° patch at the fovea with 400 x 200 sampling points and conventional post processing. A 16° patch with a total of 800 x 400 sampling points after applying spectral splitting is depicted in Fig. 19 (b). In order to appreciate the improvement in sampling we extract the 8° patch out of Fig. 19(b) and plot it in Figure 19 (c). One can visually verify, that the 8 ° selection of the 16° patch given in Fig. 19 (c) with 400 x 200 sampling points exhibits the same structure and information as the one obtained with the conventional 100 kHz processing in Figure 19 (a). There is moreover a noticeable improvement in contrast for the split spectrum method for the same reason as discussed for figure 18. In figure 19(b) we observe a decrease of contrast and higher spurious bulk signal towards the nasal side at the superior and inferior edge of the angiography.

This is an artifact that results from the higher signal backscattering from the retinal nerve fiber layer. Such artifacts need to be carefully considered when interpreting intensity based OCT angiographies.

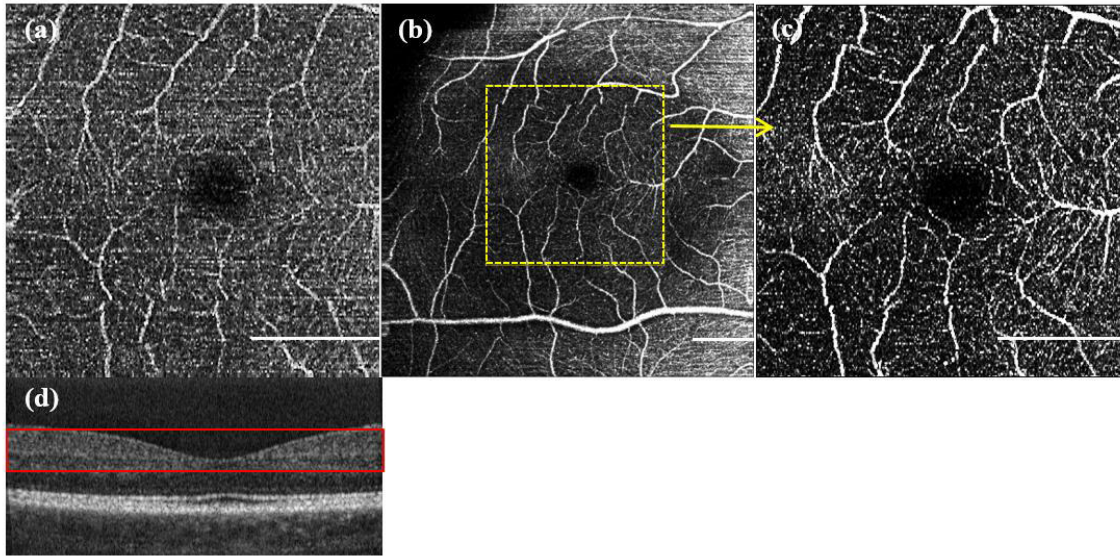


Figure 19, (a) showing a 8° section around the Fovea with a standard 100 kHz SS-OCT. (b) shows the 16° double FOV with the 400 kHz approach, in (c) the 8° section of these 16° image can be seen, which shows remarkably the same structure and even a better SNR. Self-generated

In order to demonstrate the advantage of the split spectrum approach for enhanced FOV, images at the fovea region over 16° FOV are compared. Figure 20 (a) shows the angiography obtained with the multiplexed laser without spectral splitting (200 kHz), whereas Figure 20(b) shows the result obtained after splitting the spectrum (400 kHz). Applying **Eqn. 13**, the split spectrum approach offers a global increase in SNR of 2,6 dB. To further quantify the potential of this procedure, a section of microvascular structure (marked yellow in Figure 20(a) and 20(b)) was compared. The profile plot in (Figure 20(e)) allows to appreciate the increase in SNR of even 2,9 dB within the regions of interest in Fig. 20 (c) and (d).

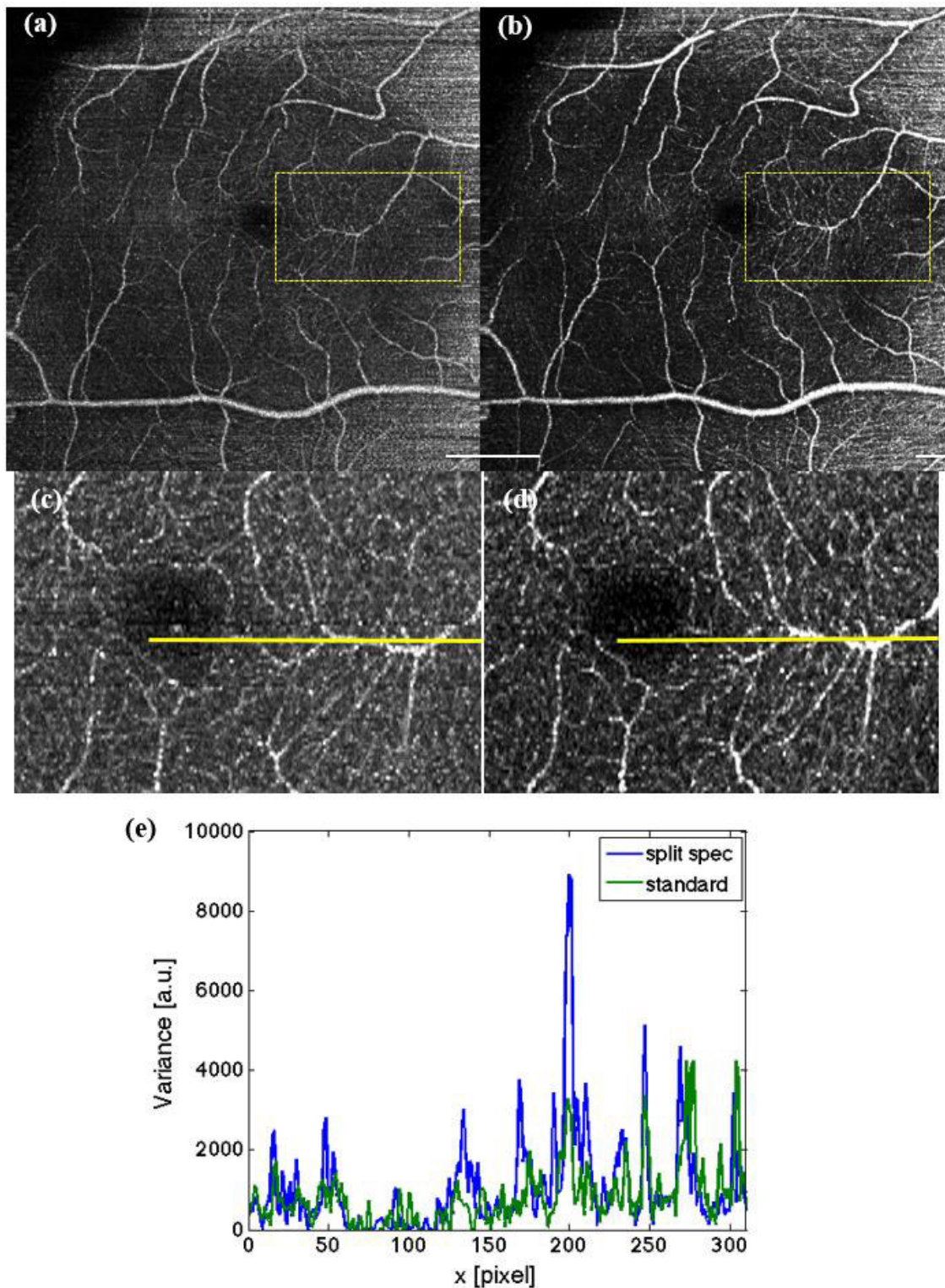


Figure 20, (a) shows the 16° Fovea section with the multiplex 200 kHz, in comparison with the (b) 16° double split technique. (c) and (d) shows the yellow subsection of (a) and (b) to clarify the quality increase. (e) Shows the line plot of this subsection (yellow line) a remarkable increase in SNR is visible. Self-generated

Finally in Figure 21 we assess the optic nerve head (ONH) region with 16° FOV of a healthy human volunteer. Figure 21(a) shows the result for the conventional processing with 200 kHz sampling rate. In comparison the higher sampling due to the split spectrum method **chapter 3** yields finer vascular details. In particular within the superior part in Figure 21(b) capillary vessels that run just below and in parallel to the nerve fiber bundles emanating from the optic nerve head are clearly visible. Assessment of the integrity of those capillaries might be of importance for glaucoma diagnostics. Obviously the loss in axial resolution does not affect the capability to visualize those fine vascular details as compared to the result in Figure 21(a) using the full optical

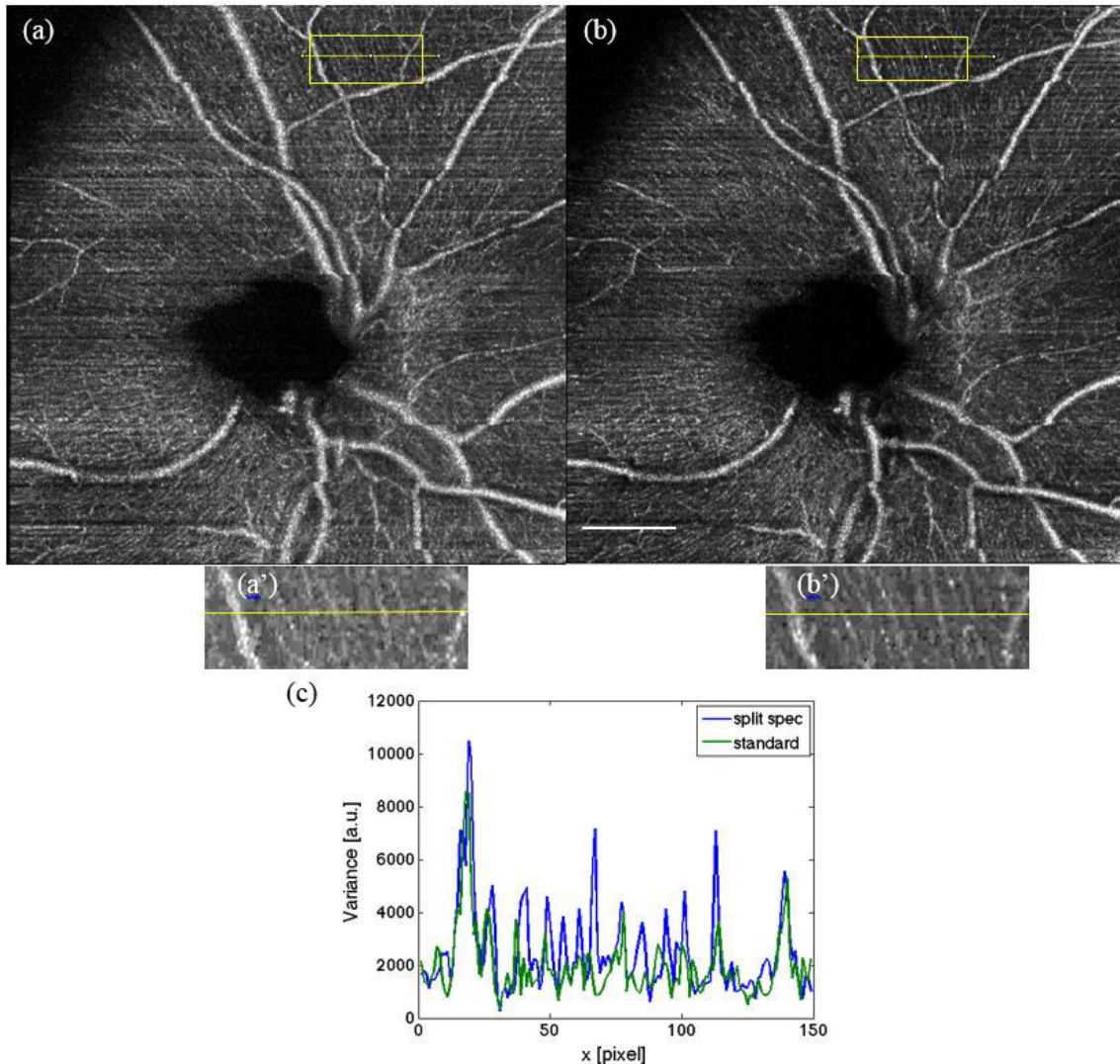


Figure 21, (a) shows the 16° ONH section with 200 kHz and (b) with the double split 400 kHz. As well there are subsections to show the increase in SNR (a') and (b'). (c) shows the line plot, again an increase in SNR is visible. Self-generated

bandwidth. Image 21(b) shows an increase of 1,4 dB in SNR compared to 21(a). The increase is lower as for Fig. 5, because the maximum projection was done over a larger number of slices, as the vascular structure at the ONH has stronger depth diversity.

In principle more than two sub-spectra could be used in order to further increase the lateral sampling. The limitation is however, the loss in sensitivity due to the loss in signal for the sub-spectra, as well as the loss in axial resolution. In our case a factor of two helped to improve the imaging performance. Further splitting did not improve significantly the performance of OCT angiography as measured by **Eqn. 13**, and would eventually lead even to SNR degradation.

4.4 Angular Compounding

For demonstrating the method of angular compounding we acquired image stacks of the fovea across a FOV of 8° and 16° and calculated the OCT angiograms with the bidirectional OCT system. Each recording consists then of two channels A/B, each of which represents a different viewing angle. Then we took maximum intensity projections over 10 en-face slices of the angiograms at the same depth from channel A and channel B. Using the information of both channels by angular compounding allows to efficiently mitigate the drawback of a dual beam device regarding the intensity reduction of each beam compared to a single beam device. To combine the images of both channels they have to be elastically co-registered due to the different viewing angle of each beam.

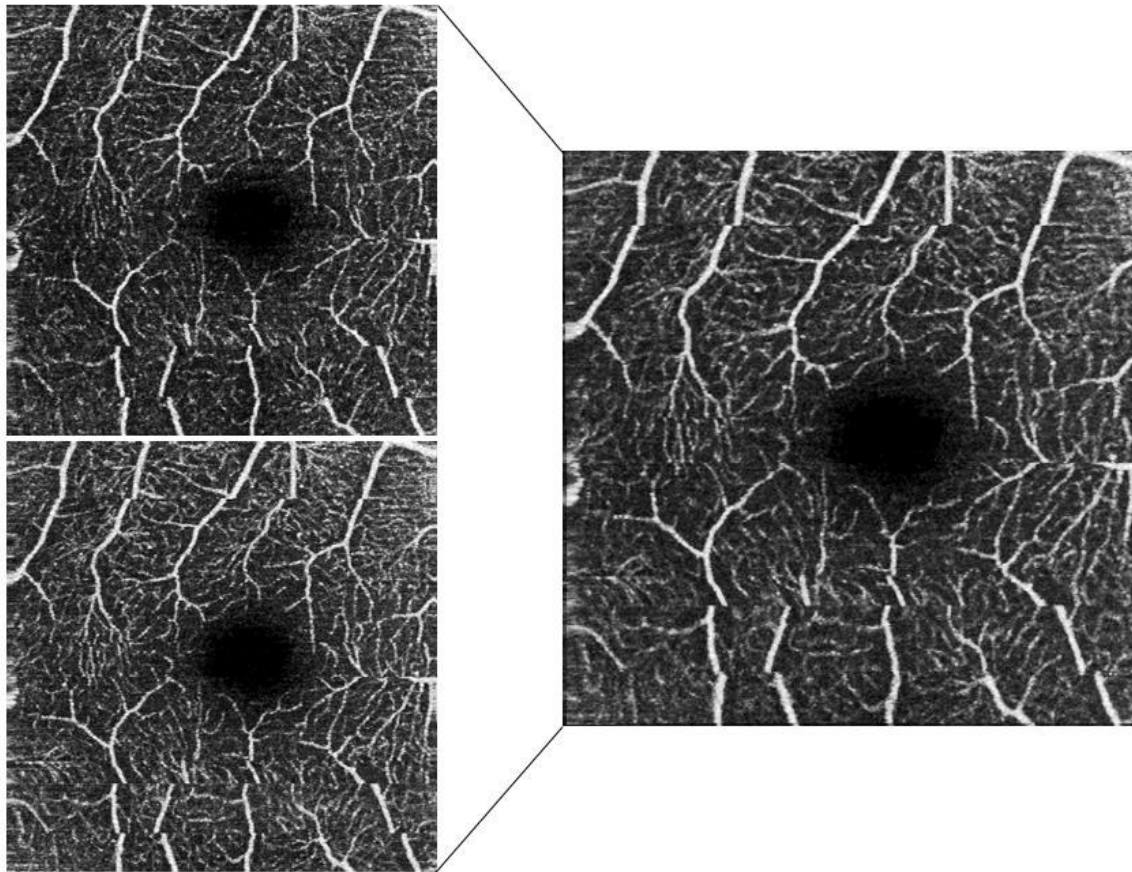


Figure 22, shows the increase in microvascular structure contrast for an image of 8° across the fovea, using angular compounding. The images of the two different beams are plotted in the left column. Each beam offers a slightly different angle to the fovea, resulting in different speckle patterns. Summation averages speckle, which improves structural details in the compounded image.

The image co-registration was obtained by applying software provided as plugin of the open source image-processing platform “Fiji” called “UnwrapJ” [16].

After application of UnwrapJ, the registered images can be averaged, which reduces speckle and enhances contrast. The presented processing is straightforward to implement, and offers a good solution for the intensity loss of a dual beam system if only a single channel was considered. Figure 22 compares the images of the single channels A and B with the angular compounded image across the fovea of 8° FOV.

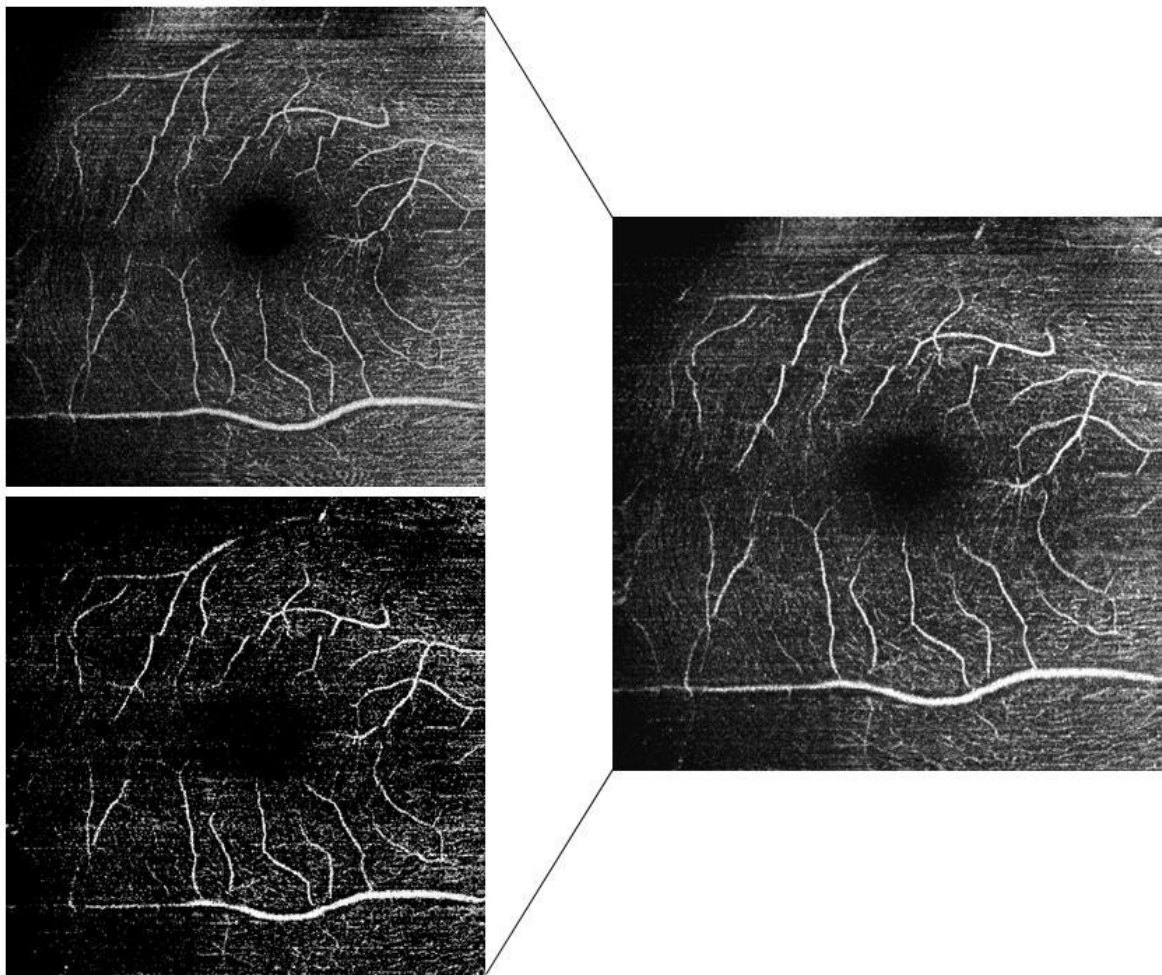


Figure 23, shows the increases in microvascular structure for a image at 16° fovea section, form the two different beams, each beam offers a slightly different vision to the fovea which improovs structural details in the compounded image.

Figure 23 shows the same region but now for a 16° FOV. It can be seen that one channel in Figure 23 has less intensity which might be due to improper alignment of the volunteer with respect to the illumination.

4.5 Case of Pathology

To demonstrate the advantage of OCT angiography for clinical diagnostics, selected patients were measured with the system. Written consent of the patient was obtained. Fig. 24 shows a case of choroidal neovascularization (CNV). The color encodes different depths, red being the retinal vasculature, and green being the choroidal vasculature. The image is obtained by stitching of two recorded volumes each across a FOV of 16° at different retinal locations.



Figure 24, shows the ONH and the Fovea of a CNV pathology, at the Fovea a neovascularization is visible (green). Self-generated

Abnormal choroidal vessel growth is well visible just underneath the fovea region. Such image can only be obtained with standard fluorescein or indocyanin green angiography, which requires administration of contrast agents. The administration bears the risk of anaphylactic shocks, which is completely absent with non-invasive OCT angiography. Furthermore it is possible with OCT angiography to visualize all retinal layers and even vasculature below the retinal pigment epithelium in the choroid. Such images are of great interest for medicals, as the CNV development can be studied. In particular longitudinal assessment of pathologies under treatment is easily obtained with OCT angiography.

5 CONCLUSION

In this thesis we implemented a new laser source to an existing dual beam OCT device. This device constructed by Cedric Blatter, had the special feature to enable rotation to the dual beam system, which makes quantitative blood flow Doppler analysis in all directions possible. This system should also enable OCT angiography by successively scanning the same position 4 times for a time of $20\mu\text{s}$. The new laser offered twice the sweeping speed compared with the old one, because it actually consists of 2 lasers sweeping vice versa. This enables double sampling, which enhances the visibility of microvascular structure. After implementing and remapping of the new laser, the images were compared with the old laser setup and an increase of 2.5 dB in SNR was analyzed.

The goal for this thesis was to enhance the FOV by keeping the same resolution compared with a 100 kHz source. This increase should be possible by increasing the speed of the source by a factor of 4 as we detect in 2 D. A new processing technique called split spectra was implemented. For this technique we split the whole spectra of the swept source, which is 105.62 nm broad at 1050 nm central wavelength. This means we get two sub spectra with 52.81 nm bandwidth. With this shorter spectrum and with a continuous scanner protocol in fast scanning, we virtually increased the scanning speed by a factor of 2. This results in doubling the frequency of the new laser source and again an increase of 2 by splitting the spectra, which leads to virtually 400 kHz sweeping frequency. This new process was used to double the 2D FOV compared to a conventional 100 kHz source. As the results show this new processing enables doubling the FOV, by keeping the same resolution. As this new processing is done in post processing, it's a good solution for all SS-OCT devices used for angiography. When we compare this new technique with the old one (100 kHz), we get an increase of 4.78 dB in SNR at the 8° section of the Fovea centralis. We managed to write a paper [17], which was published in October 2014 in the Journal of Photonics.

To further increase the quality of our images we again developed a new way to get use of our two channels. As we have a dual beam system the intensity deposited in the eye needs to be reduced for each beam. This means we lose sensitivity in comparison with a single beam system. To overcome this drawback we implemented a technique called angular compounding described above. We compared the two images of each beam and averaged it in reference to each other. This increased again the SNR and is a good solution to overcome

the drawback of a dual beam system regarding intensity adaption for each beam.

The last step in this work was the implementation of a new scanner to the system, which should reduce noise and increase the FOV as the original scanners (Thorlabs Inc) were on their limit at the necessary scanning speed for 16° FOV. For the new scanner the whole system had to be adapted, and remapped again. Due to its reduced noise, the higher Voltage supply and a better remapping the resolution of the images with the new scanners could again be increased. In general the now existing setup is a good solution to the challenges met in stat-of-the-art OCT angiography, which was always a small FOV with good microvasculature structure or a big FOV with a drop in microvasculature structure or increased acquisition time. With the described setup now the Dual beam Doppler OCT system is enabled to detect microvascular structure at a FOV of 16° which is an increase of more than double compared with the old setup using 100 kHz and the previous scanners working at their limit at 16°.

6 OUTLOOK

For this system and the angiography the post processing can be professionalized. Which means for a good angiography an exact detection of the different layer in the retina is of great importance to determine diseases and to get a proper view from layer to layer without the penetration of other layers. This is important as the medicals are used to look at en face views of the eye from the fluorescein angiograms and are yet not accustomed to look at a whole 3D stack.

Another outlook is to reprogram the image processing as it is now time-consuming and should be programmed on the GPU in C++ to enhance image processing speed to get probably to the point of real-time view of the angiography images during measurement. This could increase the quality of images as otherwise too much motion of the eye or blinking during measurement destroys good images quality.

The next step is to test a series of patients with different diseases in order to demonstrate the system performance for clinical imaging. Furthermore, for Doppler OCT the phase correlation between the two sweeps needs to be analyzed. If there is a correlation, the processing program for the quantitative blood flow needs to be adapted to get the blood flow via the phase shift caused by moving blood cells, which was described in **chapter 2**.

7 REFERENCES

- [1] Wolfgang Drexler, James G. Fujimoto, Optical Coherence Tomography, Technology and Applications, ISBN 978-3-540-77549-2 (2008).
- [2] M.A. Duguay, A.T. Mattick, Appl. Opt. 10, 2162 (1971).
- [3] Maciej Wojtkowski Institute of Physics, Nicolaus Copernicus University, Poland, High-speed optical coherence tomography basics and applications, APPLIED OPTICS / Vol. 49, No. 16 / 1 June 2010.
- [4] D. Huang, E.A. Swanson, C.P. Lin, J.S. Schuman, W.G. Stinson, W. Chang, M.R. Hee, T. Flotte, K. Gregory, C.A. Puliafito, J.G. Fujimoto, Science 254, 1178 (1991).
- [5] A.F. Fercher, C.K. Hitzenberger, W. Drexler, G. Kamp, H. Sattmann, Am. J. Ophthalmol. 116, 113 (1993).
- [6] Rainer A. Leitgeb, Current Technologies for High-Speed and Functional Imaging with OCT. Chapter 3 aus dem Buch Advances in Imaging and Electron Physics, First edition 2011, Vol. 168, pp. 109---192.
- [7] Gonzalez, R.C.; Woods, R.E. Digital Image Processing; 3rd ed., Prentice Hall: Upper Saddle River, NJ, USA, 2008.
- [8] A. S. G. Singh, "Functional Retinal Optical Coherence Tomography-Advancing Data Analysis and Exploring Holographic Imaging Concepts, 2012.
- [9] W. Choi, B. Baumann, J. Liu, A. Clermont, E. Feener, J. Duker, and J. Fujimoto, "Measurement of pulsatile total blood flow in the human and rat retina with ultrahigh speed spectral/Fourier domain OCT," Biomed. Opt. Express 3, 1047-1061 (2012).
- [10] C. Blatter, S. Coquoz, B. Grajciar, A. S. G. Singh, M. Bonesi, R. M. Werkmeister, L. Schmetterer, and R. A. Leitgeb, "Dove prism based rotating dual beam bidirectional Doppler OCT," Biomedical Optics Express 4, 1188-- - 1203 (2013).

- [11] Blatter, C.; Weingast, J.; Alex, A.; Grajciar, B.; Wieser, W.; Drexler, W.; Huber, R.; Leitgeb, R.A. In situ structural and microangiographic assessment of human skin lesions with high-speed OCT. *Biomed. Opt. Exp.* 2012, 3, 2636–2646.
- [12] http://en.wikipedia.org/wiki/Vitreous_humour#mediaviewer/File:Schematic_diagram_of_the_human_eye_en.svg (2014)
- [13] J. Reynolds and S. Olitsky (eds.), *Pediatric Retina*, 39 DOI: 10.1007/978-3-642-12041-1_2, © Springer-Verlag Berlin Heidelberg 2011
- [14] *Basicseminar_OCT_2013_7_OCTprocessing_v3* (2014)
- [15] Y. Jia, O. Tan, J. Tokayer, B. Potsaid, Y. Wang, J. J. Liu, M. F. Kraus, H. Subhash, J. G. Fujimoto, J. Hornegger, and D. Huang, "Split-spectrum amplitude-decorrelation angiography with optical coherence tomography," *Optics Express* 20, 4710-4725 (2012).
- [16] I. Arganda-Carreras, C. O. S. Sorzano, R. Marabini, J.-M. Carazo, C. Ortiz-de Solorzano, and J. Kybic, "Consistent and Elastic Registration of Histological Sections using Vector-Spline Regularization," *Lecture Notes in Computer Science*, Springer Berlin / Heidelberg, volume 4241/2006, *CVAMIA: Computer Vision Approaches to Medical Image Analysis*, pages 85-95, 2006.
- [17] L. Ginner, C. Blatter, D. Fechtig, T. Schmoll, M. Gröschl, R. A. Leitgeb. *Wide-Field OCT Angiography at 400 KHz Utilizing Spectral Splitting Photonics* 2014, 1, 369-379

8 APPENDIX

L. Ginner, C. Blatter, D. Fechtig, T. Schmoll, M. Gröschl, R. A. Leitgeb
Wide-Field OCT Angiography at 400 KHz Utilizing Spectral Splitting
Photonics 2014, 1, 369-379

Article

Wide field OCT angiography at 400 KHz utilizing spectral splitting

Laurin Ginner^{1,2}, Cedric Blatter^{1,†}, Daniel Fechtig^{1,2,†}, Martin Gröschl³, and Rainer A. Leitgeb^{1,2,*}

¹ Center of Biomedical Engineering and Physics, Medical University of Vienna, Waehringer Guertel 18-20, 1090 Vienna, Austria

² Christian Doppler Laboratory for Laser Development and their Application to Medicine and Biology, Center for Medical Physics and Biomedical Engineering, Medical University Vienna, Austria

³ Institute of Applied Physics, Technical University Vienna, Wiedner Hauptstraße 8-10/E134, A-1040 Vienna, Austria

† These authors contributed equally to this work.

* corresponding author: e-mail: rainer.leitgeb@meduniwien.ac.at
Tel.: +43-1-40400-17140; Fax: +43-1-40400-39880.

Received: / Accepted: / Published:

Abstract: Optical coherence tomography (OCT) offers the possibility to substitute retinal angiography with invasive dye administration by performing optical imaging. Besides its non-invasive character, OCT angiography offers full three-dimensional information of the retinal vasculature and has the advantage of being faster than conventional fluorescence angiography. OCT angiography is based on speckle variance, which allows calculation of the microvascular structure in the retina. However, the resolution of the angiography is strongly dependent on the number of sampling points and the acquisition speed of the OCT configuration. We demonstrate a way to gain acquisition speed and resolution by using spectral splitting with a Doppler OCT system. This allows increasing the field of view by a factor of 2 while keeping the same resolution and measurement time as compared to state-of-the-art swept source based OCT modalities.

Keywords: Optical Coherence Tomography (OCT), retinal angiography, Optical Angiography, Speckle Variance OCT (SV OCT), Swept Source OCT (SS OCT), Field of View (FOV), Doppler OCT (DOCT)

1. Introduction

The ability to substitute conventional biopsy with non-invasive optical methods was a central aim when Optical Coherence Tomography (OCT) was proposed [1, 2]. Since then, the performance of OCT devices in terms of speed, sensitivity and resolution significantly enhanced the capability of acquiring diagnostic valuable information of tissue morphology in many clinical applications. The ever increasing imaging speed, in particular mediated by swept source OCT (SS OCT) made it possible to acquire densely sampled volumes with wide field of view (FOV) without the wrecking effects of motion artifacts[3]. This development is of importance in monitoring retinal diseases at an early stage, since OCT is to date the only technique capable of assessing three-dimensional (3D) retinal morphology with μm -resolution in vivo. However, the diagnosis of retinal diseases like diabetic retinopathy, age-related macular degeneration, and glaucoma requires additional information about physiological parameters like magnitude and direction of blood flow and vascularization. Part of this diagnostic gap can therefore be bridged by Doppler OCT (DOCT) and OCT angiography [4, 5]. Recent developments in quantitative DOCT allow nowadays for a precise temporal and spatial description of the flow within individual vessels as well as of the total retinal perfusion. On the other hand, OCT angiography has been rapidly developing during the last years profiting especially from technological advancements in high speed OCT. OCT angiography images exhibit outstanding contrast even for smallest capillaries, and has the important advantage of resolving retinal versus choroidal vasculature. State-of-the-art technique for performing ocular vascular imaging is angiography using fluorescein (FA) or indocyanin green (ICGA) as contrast agents. The drawback of FA/ICGA is its time-consuming (up to 30min) and invasive character, requiring the intravenous application of contrast agents. Eventual side effects include allergic shock, nausea, vomiting or multiple painful needle sticks. This prohibits repeated examinations of patients or the screening of large populations, which would be advantageous for early detection of vascular related diseases. Moreover, these techniques cannot provide depth information and are limited by the two-dimensional (2D) nature of the images [6]. OCT angiography has the potential to provide vascular contrast in a depth resolved manner, with high resolution, and in without the need of FA/ICGA administration. OCT angiography may be used to diagnose diseases related to ocular vascularization like glaucoma, diabetic retinopathy, and age-related macular degeneration (AMD), which are the leading causes of blindness in the industrialized world. The combination of both, DOCT and OCT angiography therefore offers important biomarkers for disease diagnosis that are currently not available, mainly due to technological reasons.

In general OCT angiography can be performed via inter B-scan speckle or phase fluctuation analysis. Moving red blood cells cause signal fluctuations that can be easily contrasted against the static signal of bulk tissue using variance techniques. Speckle variance is particularly easy to implement for swept source OCT, as it remains unaffected by trigger jitter[7]. The applied contrast algorithm for OCT Angiography is based on calculating the squared logarithmically scaled intensity differences of N successive tomograms taken at the same vertical location[8]. With $I(\mathbf{x}, \mathbf{y}, \mathbf{z}) = 20 \cdot \log[|FFT(I(\mathbf{x}, \mathbf{y}, \mathbf{k}))|]$ being the tomograms and $(\mathbf{x}, \mathbf{y}, \mathbf{z})$ being the respective slow scanning, fast scanning, and depth coordinate. The differences are written as $\mathbf{D}(\mathbf{x}, \mathbf{y}_i, \mathbf{z}) = [I(\mathbf{x}, \mathbf{y}_{i+1}, \mathbf{z}) - I(\mathbf{x}, \mathbf{y}_i, \mathbf{z})]^2$, where the index i runs over the tomograms taken at the same vertical position. The

intensity difference tomograms D exhibiting high decorrelation are rejected by comparing their respective mean value to a threshold T according to the procedure described in [9]. The final motion contrast volume P is obtained by averaging over the after thresholding remaining intensity difference tomograms for each vertical position. As the above described procedure indicates, the total measurement time for a full volume is increased by the redundancy factor N in comparison to the standard OCT measurement protocol. Larger N results in improved vascular contrast, but increases the in-vivo measurement duration [10]. The latter increases the probability of motion distortion, especially in case of patients with reduced visual acuity and fixation capability. This usually limits the diagnostic valuable FOV to approx. 8deg in state-of-the-art OCT angiography modalities. For achieving larger FOV stitching can be employed, which however increases the measurement session time, and calls for retinal tracking systems. Alternatively, the speed of the OCT system can be increased. However for enhancing the FOV to about 20deg and larger, as is standard for fluorescein angiography, an about 10 time faster swept source is needed. Using a laboratory prototype FDML laser operating at 1.6 MHz a 50° FOV has been demonstrated [12]. Such laser is however not easily available, which motivates the search for alternatives to increase the speed of OCT systems that employ commercially available swept sources appropriate for retinal imaging.

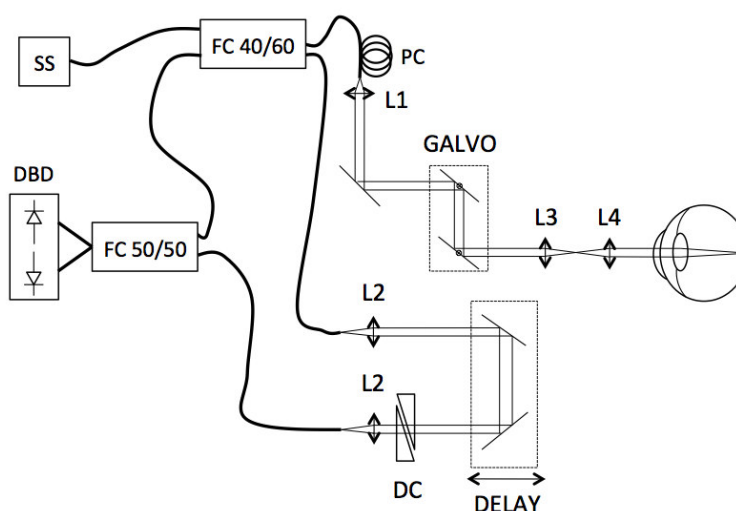
In the present work we demonstrate such method for speed-enhanced OCT angiography based on commonly available swept source technology. The laser comprises two interleaved sources, each operating at 100 kHz, and together achieving 200 kHz. To further increase the acquisition speed by a factor of 2, we propose a method based on splitting the optical spectrum. The split-spectrum approach was proposed by Jia et al to improve the signal-to-noise-ratio (SNR) of the OCT angiography images by relaxing the sensitivity to bulk motion noise in axial direction [11]. Our attempt allows for doubling the FOV from 8° (100 kHz) to 16° (400 kHz) without the need of increasing the total measurement time and keeping vascular structural integrity. The performance is demonstrated in-vivo at different locations of the human retina.

2. Basic Technology of OCT Angiography

2.1. System

The OCT system setup is displayed in Fig. 1. The light source is a commercially available swept source (SS)(AXSUN A13000467) operating at 200 kHz sweep repetition rate with spectral output centered at 1050nm. The source has an optical bandwidth of 110nm with an axial resolution in tissue of 5 μ m. The interference is measured with a dual-balanced detector (DBD) (PDB430C, Thorlabs). The signal is digitalized at 250MSamples/s with a 12bit analog-to-digital converter (ATS9350, Alazartech). The total power at the cornea is ~1.2mW, which is consistent with the ANSI standards safe exposure limits, leading to a measured sensitivity of ~94dB. The telescope (L3,L4) in the sample arm has an angular magnification of 1.5x. With a beam size of ~1.3mm at the cornea, the theoretical spot size on the retina is 25 μ m.

Figure 1, Schematic of SS DOCT setup: SS-swept source, FC-fiber coupler, PC-polarization controller, DBD-dual balanced detector, DC-dispersion control, L1-L4-achromatic doublets;



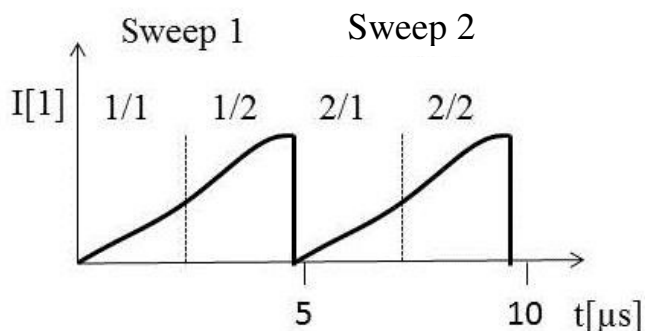
2.2. Principle of OCT angiography utilizing spectral splitting;

As explained in the introduction OCT angiography is based on observing signal decorrelation due to moving red blood cells within vessels. OCT angiography based on swept source OCT is easily obtained by assessing speckle decorrelation [7]. The present SS OCT system (Fig. 1) is equipped with a swept source laser, consisting of two multiplexed lasers, each operating at 100 kHz with a duty cycle of about 48%. When the forward sweep (Sweep 1) of the first laser is done, the corresponding back sweep is suppressed and the second laser starts the respective forward sweep (Sweep2) and vice versa (figure 2). Thus, the duty cycle can reach nearly 100%, yielding an effective sweep frequency of 200 kHz. To further increase the imaging speed of the system, we split the measured optical spectra into two halves (Fig. 2). If combined with continuous lateral scanning, the lateral sampling rate is thus improved by a factor of two to 400kHz. Prior to performing the Fast Fourier Transform (FFT) of the spectral data, the two split spectra are multiplied with a Hanning window.

The splitting offers the possibility to double the A-scan frequency of our system from 200kHz to 400 kHz, which again doubles the amount of sampling points without the need of changing the system acquisition parameters. Consequently, the FOV can be increased by a factor 2 in both lateral dimensions as compared to a single laser system operating at 100kHz. Note, that this method requires a

continuous scanning protocol of the fast axis galvo scanner (e.g. a linear ramp driving signal) in order to effectively increase the sampling rate. In contrast, a step-scan protocol would not affect the lateral sampling rate, since the split spectra (Split 1/1 and Split 2/1 in Fig. 2) would both correspond to equal lateral scanner positions.

Figure 2, Sweep structure of the multiplexed laser showing the interleaved sweeps of first and second laser as described in the text. Sweep 1 and 2 are split into sweep 1/1, 1/2 and sweep 2/1, 2/2, respectively. I is intensity of the acquired spectrum, t is the time of sweep duration.



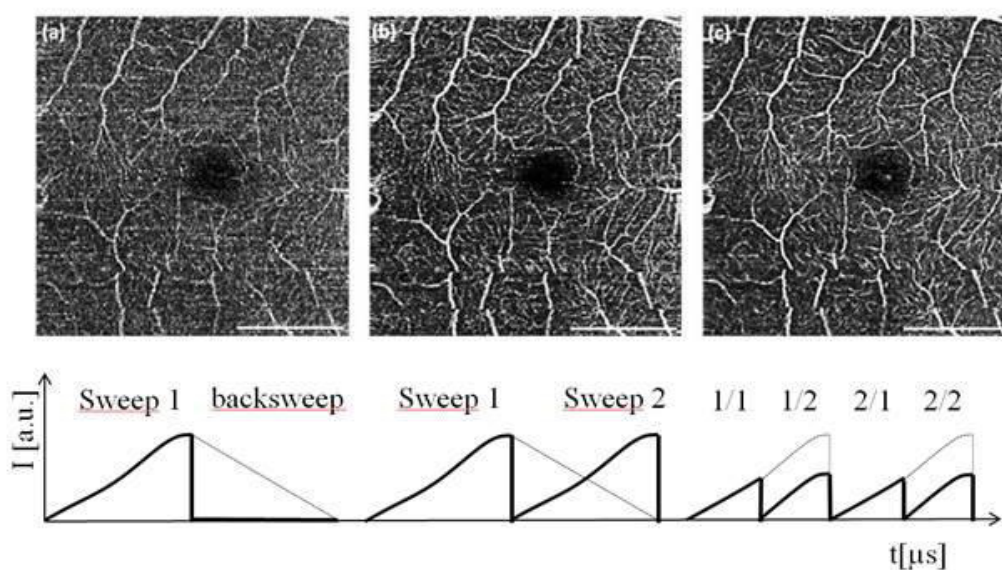
Utilizing the spectral splitting method reduces the axial resolution due to a decrease in spectral bandwidth $\Delta\lambda$. The operating laser emits light at a center wavelength of 1049.72 nm and a respective bandwidth of 150.62 nm at each sweep. Due to the splitting process, the available bandwidth reduces to 75.31 nm, hence the axial resolution is reduced from $\sim 5 \mu\text{m}$ to $\sim 10 \mu\text{m}$. This loss in axial resolution can be accepted for OCT angiography, as it is of the order of small capillary diameters and furthermore still better than the lateral resolution.

3. Results and Discussion

To demonstrate the feasibility of the split spectrum method for increasing the sampling density, we compare 8° and 16° patches acquired at 400 kHz (multiplexed laser, spectral splitting) to patches acquired at 100 kHz (single sweep laser, full spectrum) at the fovea region and optic nerve head (ONH) of a healthy volunteer. The x- scanner (fast axis) scans linearly whereas the y- scanner (slow axis) scans in steps with a vertical sampling of 400 steps. For OCT angiography we record $N=4$ tomograms at each sampling point in y- direction resulting in a total of 1600 tomograms per volume. The lateral number of sampling points is 200 for 100kHz acquisition, 400 for 200kHz, and 800 for the split spectrum method at 400kHz. The total acquisition time is 7.8 sec for all cases. Fig. 3 (a) shows an example of OCT angiography with single sweep acquisition at 100kHz and conventional processing obtained around the fovea centralis with a scanning angle of 8° , corresponding to a FOV of $3 \times 3 \text{ mm}$. The 2D angiographies are calculated as maximum intensity projections the across a selected depth range from the motion contrast volumes. In order to enable assessment of vascular structures at equal depth we flattened the motion contrast tomograms with respect to the highly reflective inner-outer photoreceptor segment boundary. Furthermore, we registered the intensity tomograms axially prior to motion contrast analysis. The depth range for the angiographies presented in Fig. 3 and Fig. 4 is indicated by the red box in Fig 4(d). The respective sweep structure is depicted underneath the angiography in Figure 3. A comparison with the multiplexed sweep acquisition in Fig. 3 (b) and with

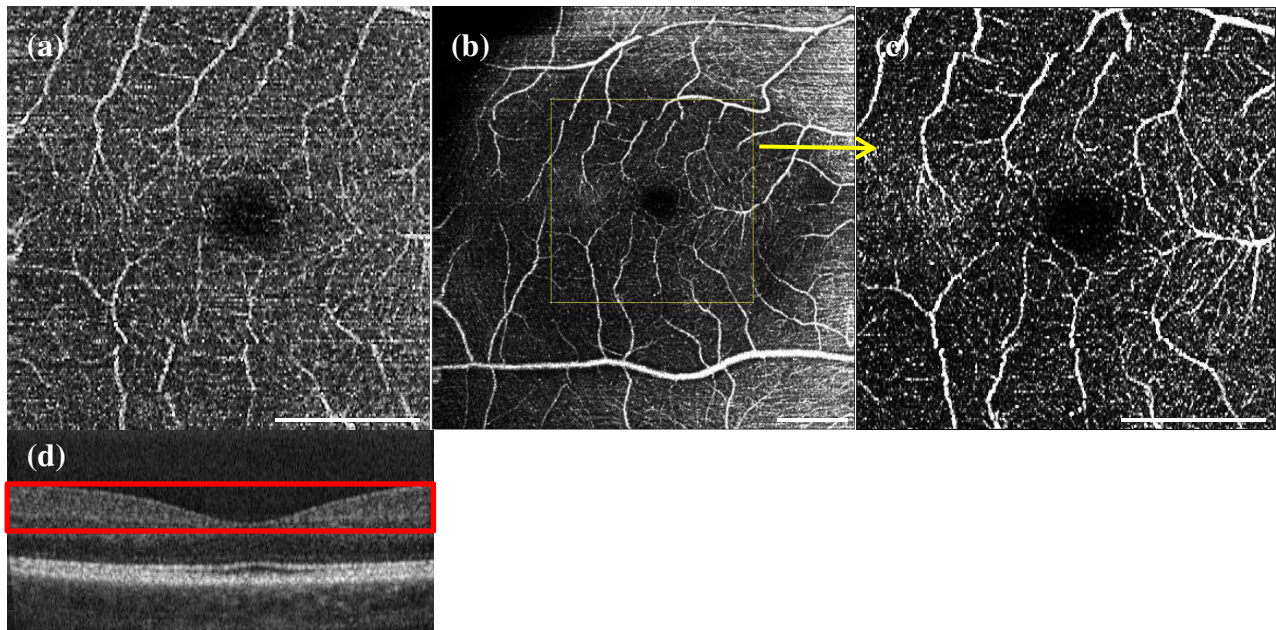
images obtained after applying the split spectrum approach demonstrates the improvement in sampling rate and thus image quality. Whereas in Fig. 3 (a) details of microvasculature are revealed only fragmentary, most of the small vessels are fully visible in Fig. 3 (b). Figure 3 (c) shows only a slight enhancement, which is due to the fact that the lateral sampling of the vessel structure is already optimal for the FOV of 3(b). Furthermore, the split spectrum approach improves the signal to noise level in the angiographies, which was already demonstrated in [11] by introducing the decorrelation signal to noise value. This effect is attributed to the lower axial resolution after spectral splitting that helps to reduce the axial decorrelation sensitivity. The situation is however different if the FOV is increased.

Figure 3, OCT angiography of the fovea for 8° FOV: (a) single sweep (100 kHz) without applying the split spectrum approach, (b) multiplex sweep (200 kHz) without applying the split spectrum approach. (c) result with multiplex sweep and split spectrum procedure. A schematic of the spectral sweep structure as a function of sweep time is shown underneath the respective OCT angiography. The white scale bar denotes 1mm.



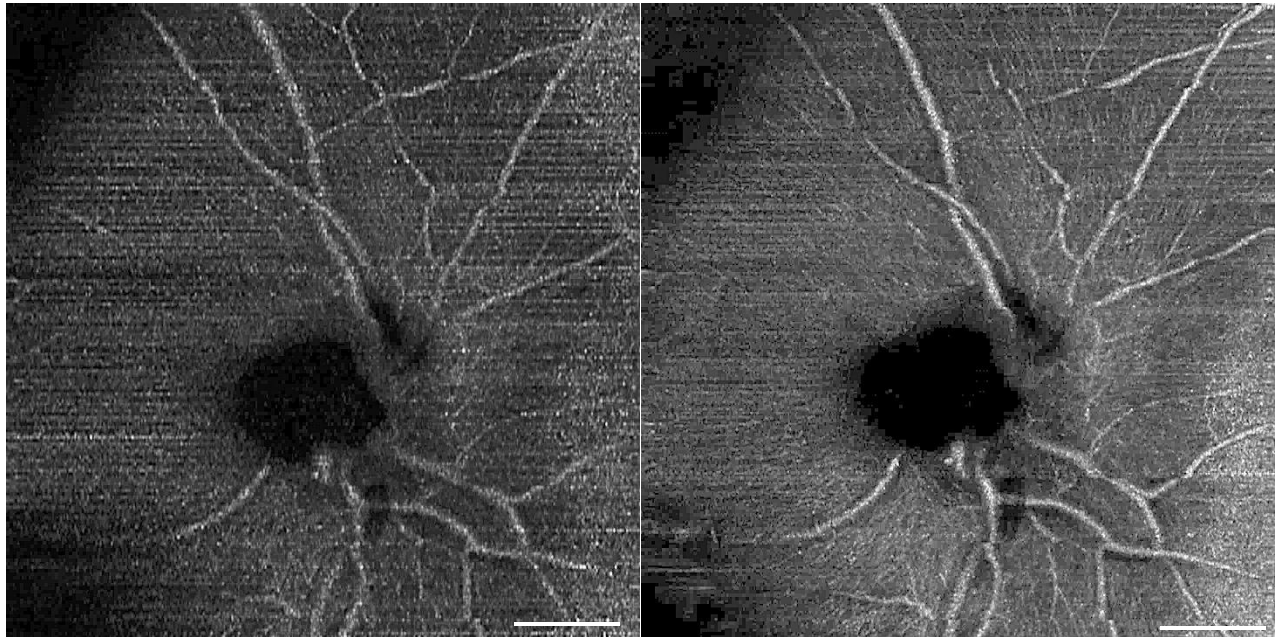
The increase of total sampling points by a factor of 4 allows increasing the FOV from 8° to 16° in both, x- and y- direction without sacrificing sampling density and measurement time. Fig. 4 (a) shows a 8° patch at the fovea with 400 x 200 sampling points and conventional post processing. A 16° patch with a total of 800 x 400 sampling points after applying spectral splitting is depicted in Fig. 4 (b). In order to appreciate the improvement in sampling we extract the 8° patch out of Fig. 4 (b) and plot it in Fig 4 (c). One can visually verify, that the 8 ° selection of the 16° patch given in Fig. 4 (c) with 400 x 200 sampling points exhibits the same structure and information as the one obtained with the conventional 100 kHz processing in Fig. 4 (a). There is moreover a noticeable improvement in contrast for the split spectrum method for the same reason as discussed for figure 3. In figure 4(b) we observe a decrease of contrast and higher spurious bulk signal towards the nasal side at the superior and inferior edge of the angiography. This is an artifact that results from the higher signal backscattering from the retinal nerve fiber layer. Such artifacts need to be carefully considered when interpreting intensity based OCT angiographies.

Figure 4, 8° with conventional 100 kHz in (a), 16° scan at fovea centralis with virtually 400 kHz (b) and 8° sub region of (b) in (c). The white bar in the right corner is 1mm in length. (d) shows the depth region of the fovea for calculating the maximum intensity projections .



Finally in figure 5 we assess the optic nerve head region with 16° FOV of a healthy human volunteer. Fig. 5(a) shows the result again for the conventional processing with 100kHz sampling rate. In comparison the higher sampling due to the split spectrum method in Fig 4(b) yields much finer vascular details. In particular within the superior part in Fig 5(b) capillary vessels that run just below and in parallel to the nerve fiber bundles emanating from the optic nerve head are clearly visible. Assessment of the integrity of those capillaries might be of importance for glaucoma diagnostics. Obviously the loss in axial resolution does not effect the capability to visualize those fine vascular details as compared to the picture in Fig 5(a) using the full optical bandwidth.

Figure 5, 16° OCT Angiography at optics nerve head: (a) with 100 kHz and conventional processing; (b) with 400 kHz using the split spectrum method. The white scale bar denotes 1mm.



4. Conclusion

In this paper, we demonstrated that the lateral sampling rate of OCT angiography can be doubled by splitting the acquired optical spectrum into two temporally equidistant halves. To evaluate the feasibility of our method for diagnostic applications in ophthalmology, we presented in vivo results of imaging healthy volunteers at the fovea and the ONH region. Those regions are of particular interest for assessment of major retinal diseases. Employing in addition a multiplexed laser, consisting of two independent interleaved source, each operating at 100kHz, we were able to quadruple the scanning speed of OCT angiography to 400kHz as compared to a single sweep laser. The lateral FOV could then be increased from 8° to 16° without the need of increasing the measurement time and without degradation in image quality and information content. Rather it additionally helped to increase the SNR of the contrasted vascular structure, since splitting the spectrum reduced axial resolution and thus sensitivity to axial sample motion during acquisition.

Diagnostic devices dedicated for the usage in daily clinical routine should be kept as simple and economic as possible. The split spectrum method is purely performed in post-processing hence it does not require any additional expenses, improvements and changes in complexity regarding the optical setup. A possible trade-off in specific applications might be the degradation in axial resolution owed to the reduction in available optical bandwidth after splitting the spectrum. This has however been demonstrated to be of no relevance for visualizing the retinal vascular structure.

Acknowledgments

The financial support by the Austrian Federal Ministry of Economy, Family and Youth and the Austrian National Foundation of Research, Technology, and Development is gratefully acknowledged. We further gratefully acknowledge instrument support by Prof. Ursula Schmidt-Erfurth.

Conflict of Interest

The authors declare no conflict of interest with respect to the content of the present research paper.

References and Notes

1. A. F. Fercher, "Ophthalmic interferometry," in *Optics in Medicine, Biology and Environmental Research* Gerd von Bally, and S. Khanna, eds. (Amsterdam: Elsevier, 1990), pp. 221–235.
2. D. Huang, E. A. Swanson, C. P. Lin, J. S. Schuman, W. G. Stinson, W. Chang, M. R. Hee, T. Flotte, K. Gregory, C. A. Puliavito, and J. G. Fujimoto, "OPTICAL COHERENCE TOMOGRAPHY," *Science* **254**, 1178-1181 (1991).
3. T. Klein, W. Wieser, L. Reznicek, A. Neubauer, A. Kampik, and R. Huber, "Multi-MHz retinal OCT," *Biomedical Optics Express* **4**, 1890-1908 (2013).
4. R. A. Leitgeb, R. M. Werkmeister, C. Blatter, and L. Schmetterer, "Doppler Optical Coherence Tomography," *Progress in Retinal and Eye Research* (2014).
5. S. Makita, Y. Hong, M. Yamanari, T. Yatagai, and Y. Yasuno, "Optical coherence angiography," *Optics Express* **14**, 7821-7840 (2006).
6. M. S. Mahmud, D. W. Cadotte, B. Vuong, C. Sun, T. W. H. Luk, A. Mariampillai, and V. X. D. Yang, "Review of speckle and phase variance optical coherence tomography to visualize microvascular networks," *Journal of Biomedical Optics* **18**, 050901-050901 (2013).
7. A. Mariampillai, B. A. Standish, E. H. Moriyama, M. Khurana, N. R. Munce, M. K. K. Leung, J. Jiang, A. Cable, B. C. Wilson, I. A. Vitkin, and V. X. D. Yang, "Speckle variance detection of microvasculature using swept-source optical coherence tomography," *Opt. Lett.* **33**, 1530-1532 (2008).
8. C. Blatter, J. Weingast, A. Alex, B. Grajciar, W. Wieser, W. Drexler, R. Huber, and R. A. Leitgeb, "In situ structural and microangiographic assessment of human skin lesions with high-speed OCT," *Biomedical Optics Express* **3**, 2636-2646 (2012).
9. C. Blatter, T. Klein, B. Grajciar, T. Schmoll, W. Wieser, R. Andre, R. Huber, and R. A. Leitgeb, "Ultrahigh-speed non-invasive widefield angiography," *Journal Of Biomedical Optics* **17**, 070505 (2012).
10. A. Mariampillai, M. K. K. Leung, M. Jarvi, B. A. Standish, K. Lee, B. C. Wilson, A. Vitkin, and V. X. D. Yang, "Optimized speckle variance OCT imaging of microvasculature," *Opt. Lett.* **35**, 1257-1259 (2010).
11. Y. Jia, O. Tan, J. Tokayer, B. Potsaid, Y. Wang, J. J. Liu, M. F. Kraus, H. Subhash, J. G. Fujimoto, J. Hornegger, and D. Huang, "Split-spectrum amplitude-decorrelation angiography with optical coherence tomography," *Optics Express* **20**, 4710-4725 (2012).